Institute of Space and Aeronautical Science, University of Tokyo
Report No. 481, May 1972

Experiment of Supersonic Air Intake Buzz

By

Toshio NAGASHIMA, Tomio OBOKATA and Tsuyoshi ASANUMA

Summary: For the purpose of examining supersonic intake instability, the authors have designed a supersonic wind tunnel of blow down type, in which the test section dimension is 200 mm × 180 mm, its Mach number is 2.0, Reynolds number is about 10^7 with reference length of air intake model diameter (60 mm).

By using this supersonic wind tunnel, experiments of inlet buzz are made, where the model is all external compression type and as parameters are used the throttle ratio (T.R.) and the center body position relative to the cowl lip (θ_A). The effect of attack angle (α) is also examined.

They show that:

1) In the subcritical regime the unstationary phenomena occur and some characteristic frequencies are observed, where the transition from lower frequency to higher one happens according to the decrease of T.R., while the amplitude is fluctuated in rather arbitrary manner.

2) The motion of the bow shock wave corresponds fairly well to the pressure records, showing complicated behaviour of the boundary layer on the center body surface when it is expelled out from the cowl lip.

In addition a theory is proposed in Appendix, where calculations are made to explain some buzz characteristics emphasizing two boundary conditions, the front shock wave and the rear choked exit.

1. INTRODUCTION

With the advancement of supersonic aeronautical engineering there has become possible airplanes fly into the supersonic speed range with their adequate installation. Speaking of supersonic air intake, the first research aiming its practical application was begun by Kl. Oswatitsch [*1*] for missile designs at the background of World War II. At Göttingen he performed wide range of experiments from simple pitot type to multishock diffuser, first demonstrating the effectiveness of external compression inlets. His experiments, however, were mainly for missile and not for airplane, distinguished from the former one by the requirement of a large operating range of Mach number and stability of air stream. In the U.S. independent work has been done by A. Ferri et al. [*2*] so much in the course of all external supersonic compression. Until then, there has been concluded that internal supersonic compression air intake has abrupt change in pressure recovery with hysterisis manner according to Mach number. Therefore, it was desired by A. Ferri et al that better results could be obtained with external supersonic com-

pression type diffuser.

The performance of supersonic air intake should be viewed from various sides connected tightly one another, for example, 1) high pressure recovery 2) minimum external drag 3) delivery of steady and uniform air into following component of the installation, etc. Concerning about the steadiness of the flow in supersonic diffuser, there have been observed many non-stationary oscillations of various amplitude, one of which undergoes violent shock excursions in and out from the cowl lip and sometimes leads to serious structural or engine operation problems.

The main interests in this report consist in the non-stationary flow phenomenon of supersonic air intake, that is, INLET BUZZ, which will be helpful for better understanding of the problems required in practical application with the frequent use of supersonic air intake for civil transportation. The main feature of inlet buzz exists in the non-stationary shock movement passing through three characteristic flow regimes, the subcritical, the critical, and the supercritical one. It seems natural, therefore, to examine for each regime the flow pattern including the unstable shock waves.

Further, if we are to try to simulate our experiments to the actual ramjet model testing, the instability arising from the combustion rear of the inlet should be taken into consideration. In this report, however, we concern only about the cold flow, that is, no burning case, because it will be better to exclude the complicated heat problems in this stage of approaching to the inlet buzz mechanism.

The purpose of our experiment is to obtain general characteristics of inlet buzz, making measurement of frequency and amplitude of pressure fluctuation and visualizing the flow patterns ahead of the cowl lip. As a new aspect of experiments, special interests will be payed to the correspondence between shock wave movement and pressure fluctuation behind it, where we shall emphasize the initial characteristics of buzzing. In addition the effect of attack angle will also be discussed.

2. Previous Investigations About Inlet Buzz

General characters of 'buzz' phenomenon up to date are prescribed as follows.

In an external compression inlet operating steadily at critical or subcritical regime, there occurs sudden normal shock jump upstream from the cowl lip, which becomes then stationary at a certain point on the center body surface. This shock location is an unsteady one, so that it returns back downstream to the cowl lip at a slower speed than before. At this time the retreating normal shock passes through the throat section, and then fierce pressure variation is initiated in the rear plenum chamber. This supercritical condition is also so unstable that the shock is again expelled out from the diffuser. Thus this oscillation is maintained as a cyclic one, but such shock movement occurs in fairly arbitrary way from experiments to experiments.

As for the parameters relating the phenomenon, basic aerodynamic parameters, such as P, ρ, T, a, μ, must be clear. We remined here only upon Mach number

and Reynolds number, which are given from the wind tunnel condition.

The utmost stress should be payed about the geometrical parameters and their meanings considering the very effect on buzz characteristics, that is, basic cycle of shock wave excursion accompanying high amplitude and low frequency pressure fluctuation at the rear plenum chamber. There come into sight the model diameter and length, the semi-appex angle of the center body, the inclination of straight line from the appex of the center body to the cowl lip, the inclination of inner wall of the cowling, etc.

We first have to determine which parameters we should stress upon, where the information from the previous experiments by many workers will give us precious stone.

The intake experiments of internal compression type, were made by A. Kantrowitz [*3*], who developed later the theory of stability and formation of normal shock wave in channel [*4*]. As described above, Kl. Oswatitsch made a wide range of experiments about the intakes for missile use [*1*], where he first demonstrated the oscillation regarded as Inlet Buzz. And A. Ferri examined the efficiency and characteristics of spike type inlet for airplane [*2*]. As for supersonic inlet stability, the origin of instability was given by A. Ferri and L. M. Nucci [*5*], which is known as Vortex Sheet Theory. Other experiments were made by C. L. Daily pointing the frequency characteristics and the separation on the center body causing to the inlet choke [*6*].

There are a large number of references concerning ramjet model. W. H. Sterbentz & J. C. Evvard proposed a criterion for ramjet flow pulsations [*7*] based upon Helmholtz resonator similarity and its extention to the prediction of fluctuation amplitude was done by W. H. Sterbentz & J. Davids [*8*]. On the other hand an analysis by a one-dimensional characteristic theory was proposed by R. L. Trimpi [*9*] opposing Helmholtz resonator theory, and in Ref. [*10*] were discussed also by him further experimental details about nonstational characteristics of Buzz. R. Hermann, writing a volume just for supersonic air intakes [*11*] stressed the role of the second throat condition on buzz cycle.

In Appendix A we summarize these previous experiments for our use.

3. Supersonic Wind Tunnel

It is well known that supersonic intakes nowadays are so complicatedly attached as to permit the adequate control of operating condition. One of these reasons is that in external compression inlet there happens so called buzz phenomenon which is characterized by the unsteady shock wave movement through in and out the cowl lip, and the pressure fluctuations with some kinds of frequency at the rear plenum chamber. This phenomenon includes the unsteady interaction between shock wave and boundary layer, which is very complicated and so far in detail examined only experimentaly.

The designed wind tunnel is for a series of experimental investigations of such unsteady phenomena in supersonic intakes. Test section geometry is determined

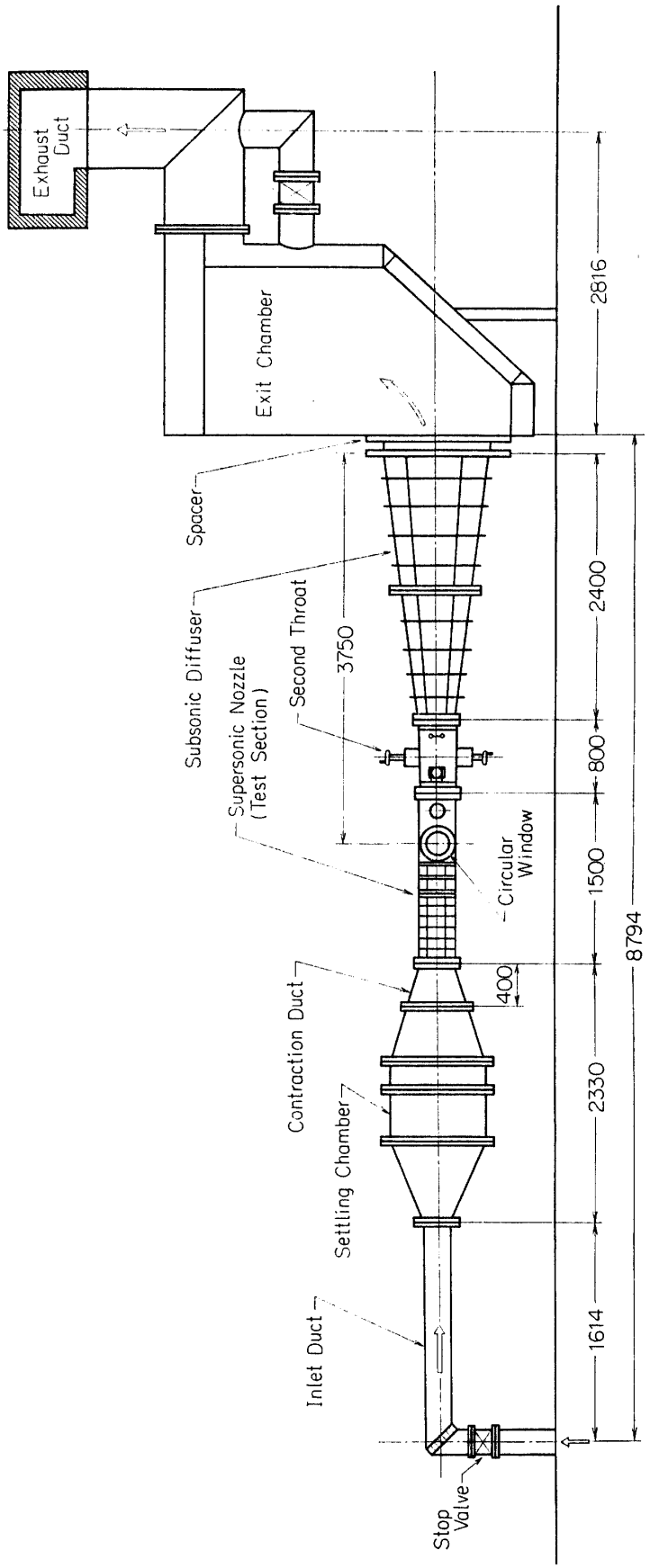

FIG. 1. General view of supersonic wind tunnel.

mainly by two conditions, the space problem of our laboratory and the reservoir capacity, so that the maximum is limited to about 200 mm×300 mm. This narrow test section has various defects, such as difficulty to assure regular supersonic stream and to change the model size for a larger one. At the stage of final decision, however, we found that the mass flow due to the specified dimension 200 mm ×180 mm of test section could be obtained only by small-mass-flow control system which have the advantage of automatic control of the settling chamber pressure, while otherwise manual control should be taken. After all, we decided that the Mach 2.0 supersonic working section and the diffuser following it must be newly constructed, but the other apparatus, such as the settling chamber and the exit chamber etc. are modified in shape or varied in location for use.

3.1 Construction of supersonic wind tunnel

The general view of our supersonic wind tunnel is shown in Fig. 1. Air is blown down from the high pressure reservoir (15 at, ~500 m^3) to our tunnel having been controlled by a small automatic control-valve. Through a settling chamber it flows into a supersonic nozzle, thus its speed becomes to Mach 2.0. Then it flows out, recovering its static pressure through a subsonic diffuser, hereafter, to an exit chamber and finally to the uniform circumference. In Fig. 2 is shown a picture of our tunnel.

According to some calculations about the features of our tunnel, its Reynolds number is about 10^7 with reference length of intake model outer diameter (D= 60 mm), the running time is 100 second for the settling chamber total pressure of 5 ata and 350 second for 3 ata, and the mass flow rate is also from 15 to 25 Kg/s and the test section pressure is 0.4~0.7 ata. Vapour condensation effect may be neglected practically, for the air is dried fairly well to drop the dew point to −40°C.

All proof systems for emergency are gathered onto a central control panel. Details are referred to [*12*]. We, here, only state that it is most preferable to

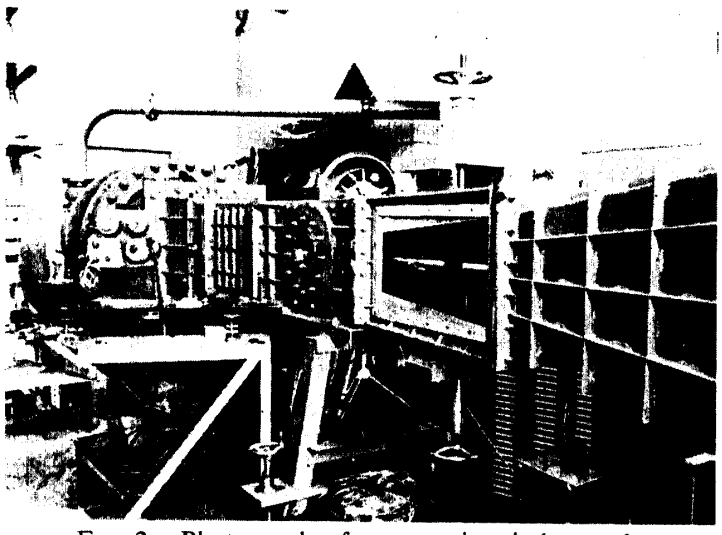

FIG. 2. Photograph of supersonic wind tunnel.

operate under the automatic control of 3.0 Kg/cm^2 balance range, 80% valve opening, which guarantees good stabilization of settling chamber pressure to 1.4 Kg/cm^2.

TABLE 1. Profile of supersonic nozzle for Mach Number 2.0

x	y
−364.22	130.00
−340.04	116.04
−325.00	110.95
−300.00	102.99
−275.00	95.67
−250.00	88.99
−225.00	82.94
−200.00	77.53
−175.00	72.75
−150.00	68.61
−125.00	65.12
−100.00	62.25
−75.00	60.02
−50.00	58.43
−25.00	57.48
0.00	57.16
5.01	57.19
55.01	58.79
105.01	62.39
155.01	67.48
205.01	73.58
255.01	80.17
273.60	82.55
393.30	84.88
313.82	87.08
335.16	89.17
357.72	91.14
381.16	92.95
405.68	94.60
431.33	96.07
457.92	97.34
485.69	98.39
514.68	99.20
544.93	99.72
576.20	100.00
⋮	⋮
1135.78	100.00

The inlet duct, the settling chamber and the exit chamber are the same that were used for tests of linear cascade of airfoils in transonic shear flow [*13*]. A contraction duct which connects the settling chamber to the supersonic nozzle is newly constructed, and the duct has an inlet section of 500 mm × 500 mm and an exit section of 180 mm × 260 mm and its length is 400 mm, as shown in Fig. 1.

The two-dimensional supersonic nozzle consists of a wooden nozzle contour and a rectangular alluminum casting alloy box containing it. Downstream it holds the test section for Mach number 2.0 and its geometry is 180 mm × 200 mm. The most important is the nozzle contour through which the flow becomes supersonic. There are many calculating methods for contour design to get uniform parallel supersonic flow. The one we applied is a simple analytic formulae. In general

TABLE 2. Position on holes measuring static pressure along nozzle contour

No.	x
1	276.5
2	329.0
3	376.5
4	433.5
5	480.5
6	530.5
7	580.5
8	630.0
9	677.5
10	727.5
11	780.0
12	827.5
13	878.0
14	929.5
15	976.0
16	1027.5
17	1075.0

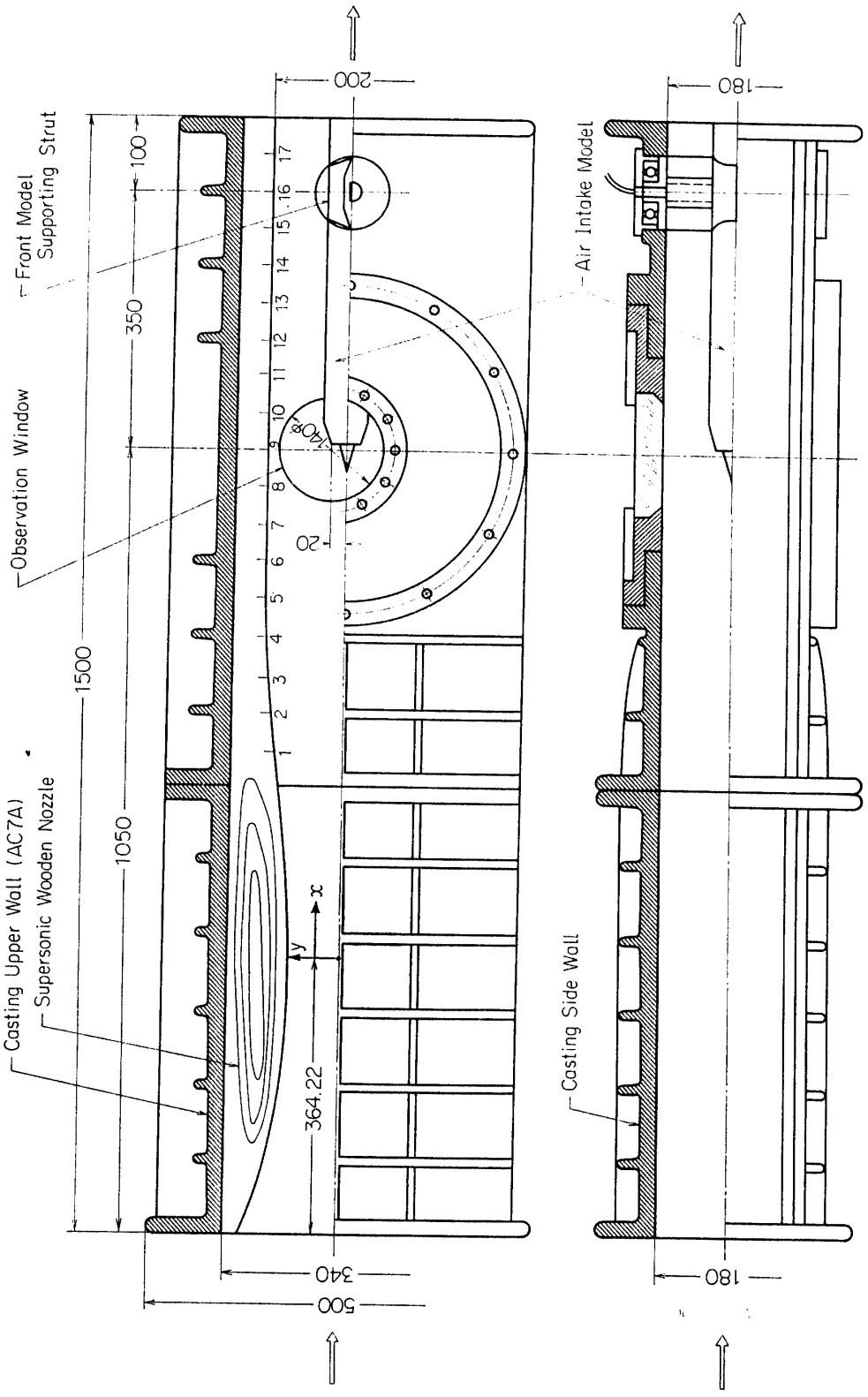

FIG. 3. Supersonic nozzle block (test section).

it is necessary to correct this contour due to the boundary layer development after the throat. This correction was made according to Tucker's method [*14*]. The profile thus determined is indicated in Table 1.

The rectangular nozzle box shown in Fig. 3 is blocked by two sets of casting walls (AC7A); upper and lower walls are firmly combined by 20 mm diameter bolts at both side walls. The wooden nozzle contour is fixed to the side walls by many screws. Calculation shows that the stress in emergency of 15 Kg/cm^2 at the throat upstream becomes 1.0 Kg/mm^2, provided the thickness of the side wall being 15 mm. Thus the safety factor is 15. Moreover, this upstream part is strengthened by many ribs 80~100 mm apart, 10 mm thick and 30 mm high. As for the downstream part the static pressure difference between outer and inner side of wall is at most 0~2 Kg/cm^2. However we use 15 mm thick walls as before, mainly considering the vibrationproof requirement of the block during blowing down.

Static pressure holes of 0.8 mm ϕ are opened at the lower nozzle contour, 8 points each upstream and downstream from the center of circular window, the total being 17 holes, whose positions are tabulated in Table 2.

As shown in Fig. 3, a pair of observation windows is attached at the side walls for Schlieren photographical techniques. The window glasses are well polished and have the thickness of 18 mm. Window center does not coincide with the frame's center for observating the flow pattern around the model with some angle of attack.

The nozzle block is followed by the second throat block, where the inlet rectangular 180×200 mm section is widened to the exist 260×340 mm as shown in Fig. 4. This block with the rear model supports is setted for the purpose of taking in or out the model from the test section, so that the whole side walls can be removed in assembling the model. Then follows the subsonic diffuser with semidffusing angle of ~7 degree, which can be divided into two of equal lateral length. The rear part is fixed to the exit chamber at its end, with the intermediate of 150 mm length spacer.

3.2 Characteristics of supersonic wind tunnel

To examine the newly constructed supersonic wind tunnel, it is planned to make, first of all, the ascertainment of the start of supersonic flow and its approximate Mach number, by measuring the longitudinal distribution of static pressure on the nozzle contour along the tunnel axis. The second step is to obtain rather accurate pressure distribution of core flow of the working section.

Throughout the experiments the pressure was measured by mercury U type manometer almost all at a time. In addition the settling chamber static pressure was continuously watched by a pressure pick-up of strain gauge type while completing each experiment.

The start of supersonic flow is ascertained by using a test model with semispherical head installing 7 pressure holes in alignment 15° apart of azimuth angle each other. In Fig. 5 there are presented the comparison of the pressure distri-

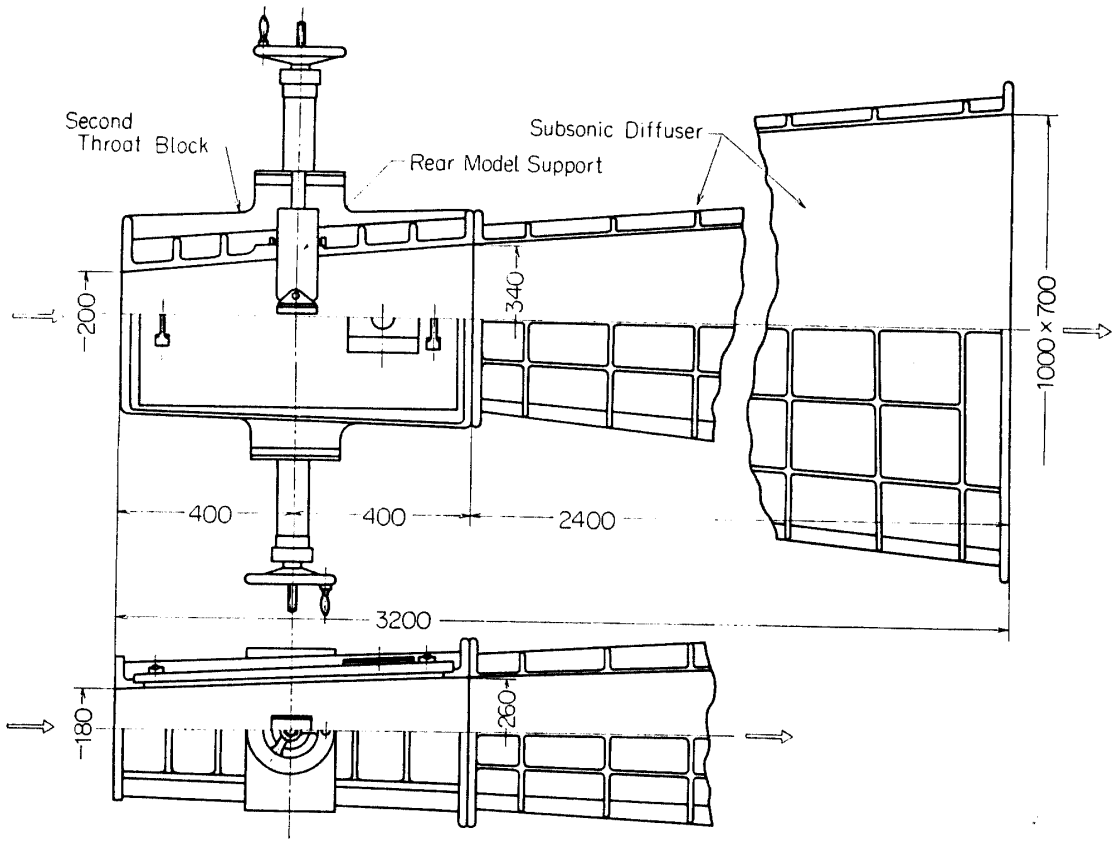

FIG. 4. Second throat block and subsonic diffuser.

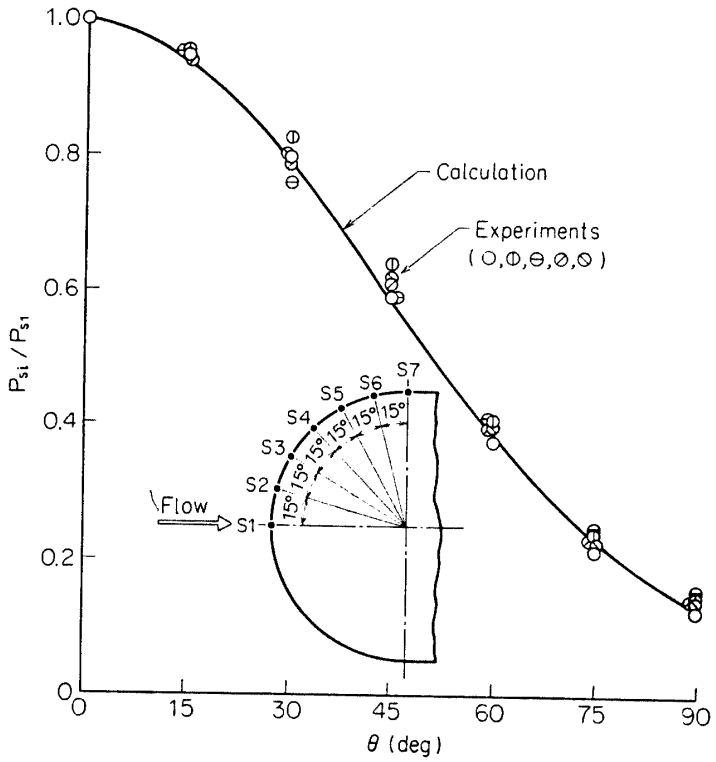

FIG. 5. Comparison of pressure distribution on semispherical head for checking of Mach number.

bution on the spherical surface between our experimental results and the theoretical points calculated by O. M. Velozerkobski [*15*]. The detached shock contour, replotted from the Schlieren photographs, is compared with the theoretical one calculated also by Velozerkobski in Fig. 6. These comparisons are in so excellent agreement that the experiments are found to show the ascertainment of the start of supersonic flow and its measured Mach number is very close to 2.0, that is between 2.04 and 1.94, estimating from the results shown in Fig. 5 and 6.

On the lower surface of the working section there are installed 17 static pressure holes and we have also three holes on the lower surface of the second throat block and the subsonic diffuser section. Thus, measuring static pressure at each point, we can describe the actual flow feature occuring in the wind tunnel, as shown in Fig. 7. Thus it may be sure that the flow is almost uniform up to the section of 150 mm downstream of the window center.

As for the important characteristics of the core flow at the working section, we employ two instruments, a static pressure tube and a total pressure tube. With

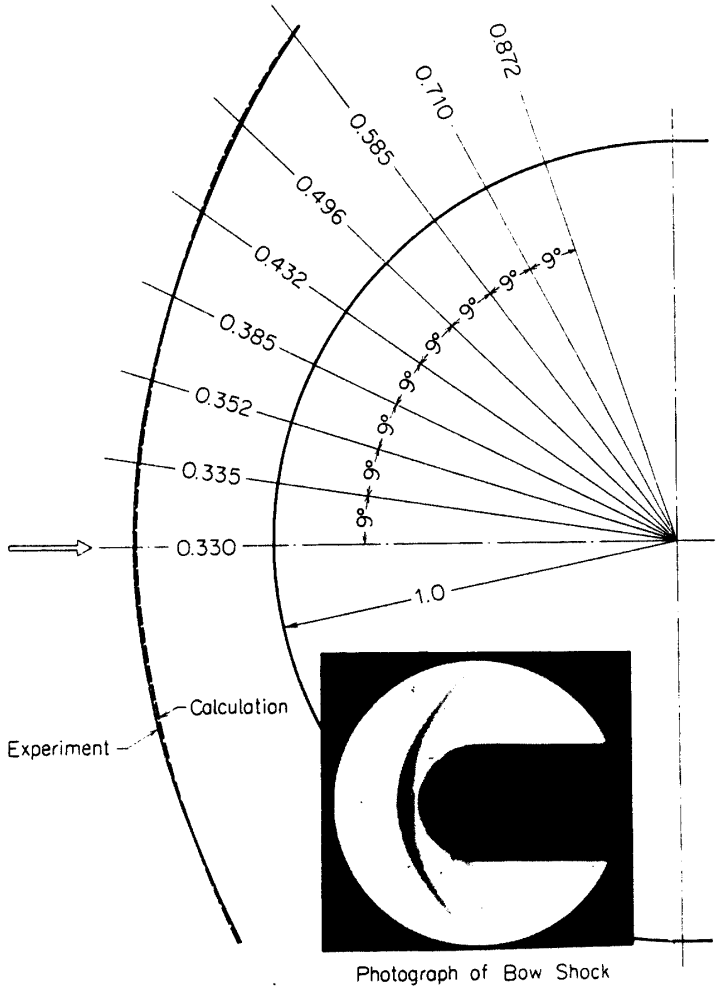

FIG. 6. Comparison of detached distance of shock wave from spherical surface.

the help of the former one we can make the measurement of longitudinal static pressure distribution for the range of 300 mm along the center line giving the exact longitudinal Mach number distribution of the core flow, while the latter enables us to make a rough estimation of area ratio of uniform core flow to the cross sectional area of the working section. As shown in Fig. 7, the static pressure distribution gives us that the core flow is fairly uniform along the wind tunnel axis. Finally we decide the actual Mach number of this wind tunnel as 1.99, regarding the results from static pressure distribution along the center line.

4. Air Intake Model

4.1 Model configuration

In order to construct an air intake model we have to determine the following geometrical parameters, such as length (L), outer diameter (D), semi apex angle of center body (θ_s), inclination between center body apex and cowl tip (θ_A), cowling wall inclinations (δ_c & ϕ_1) and center body outer wall inclination (ϕ_2) etc., which are shown in Fig. 8. It is predicted that the increase of L/D ratio leads to the increase in pressure fluctuation and the decrease in oscillating frequency. As for θ_s, the flow separation is likely to be occurred in increasing the angle. θ_A determines whether the flow is smooth or not at the cowl lip that will be connected with the efficiency of the intake. If the critical regime is established, this condition corresponds to no reflection of an oblique shock issuring from the apex of the center body.

At first, the main parameters are determined as follows: $L/D=15$ and $\theta_s=25°$

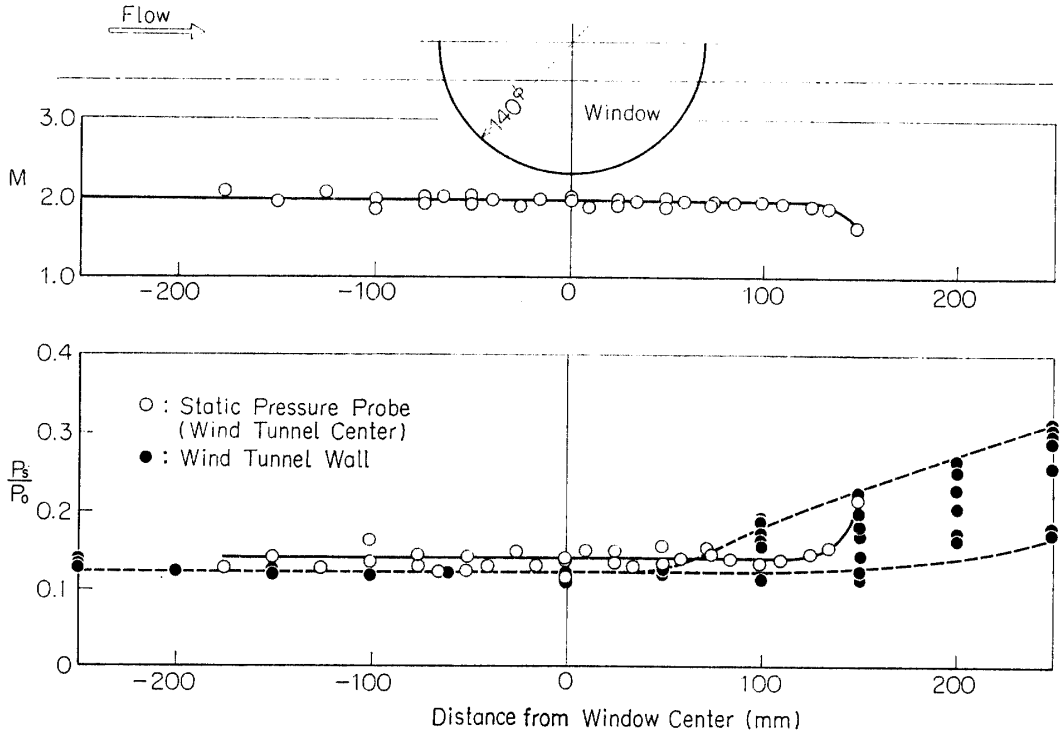

Fig. 7. Static pressure and Mach number distributions along the wind tunnel axis.

with reference to the models in previous publication about intake instability as tabled in Appendix A. Then the model diameter is determined as D=60 mm considering the wind tunnel starting problem. Thus the area ratio of intersecting area of the model to the wind tunnel test section (180×200 mm) becomes 0.0786, which may be satisfactorily small enough for the excessive value of 0.407 for the choking of the tunnel test section.

Referring to various parameters which seem to govern the unsteady phenomena of inlet buzz, there have been discussed some basic ideas about model construction. First, the fluctuating pressure is to be measured by strain gauge type pressure indicator of the least geometrical size of 6 mm dia. Second, the exit throttle valve is controlled by an electric motor to vary the exit area (A_E) continuously. Third, the center body is to be displaced by inserting medial spacer of proper length to change the inclination between the center body apex and the cowling tip (θ_A).

With these three basic ideas the model is designed. The model is divided into two main parts as follows:

The front part: As shown in Fig. 9, the leading part of the outer cylinder, that is called as cowling, must hold the center body mediated by a set of struts, which consists of two pairs of plates with 2 mm and 4 mm in thickness respectively. The thicker pair is holed for each center by 2 mm thick 12 mm long rectangular form because the lead wires originating from the pressure gauge should be taken out through this hole, thus leading to the front supporting strut of the wind tunnel. The spacers are put into the both ends of the strut ring and the center body location can be varied to and for to the amount of about 10 mm, by changing them into combination of proper pair. In our case three kinds of spacer combination are selected as indicated in Table 3.

The center body is constructed through its whole length without any intersection or joint due to the consideration of vibrational rupture and the center alignment. Some pressure indicators (P1~P3) must attach to the front end of

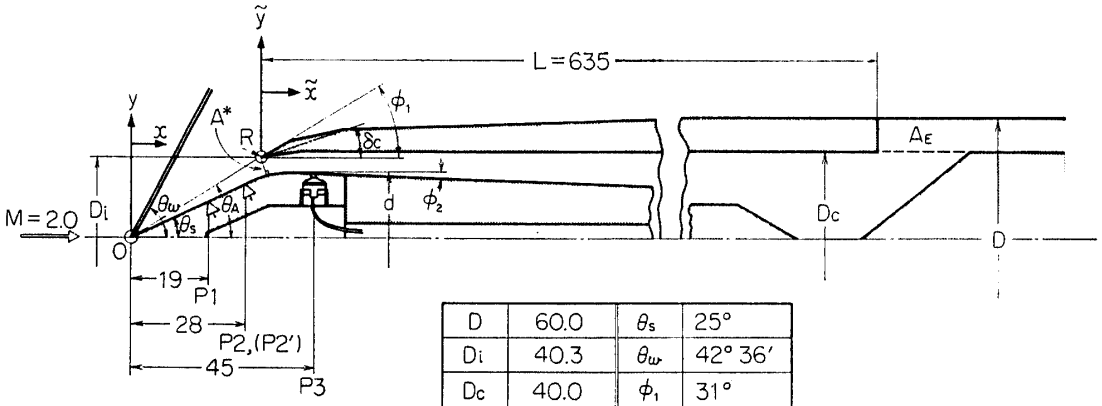

D	60.0	θ_s	25°
Di	40.3	θ_w	42° 36′
Dc	40.0	ϕ_1	31°
d	32.4	δ_c	19° 24′
R	0.05	ϕ_2	2° 18′

FIG. 8. Characteristic dimensions of air intake model.

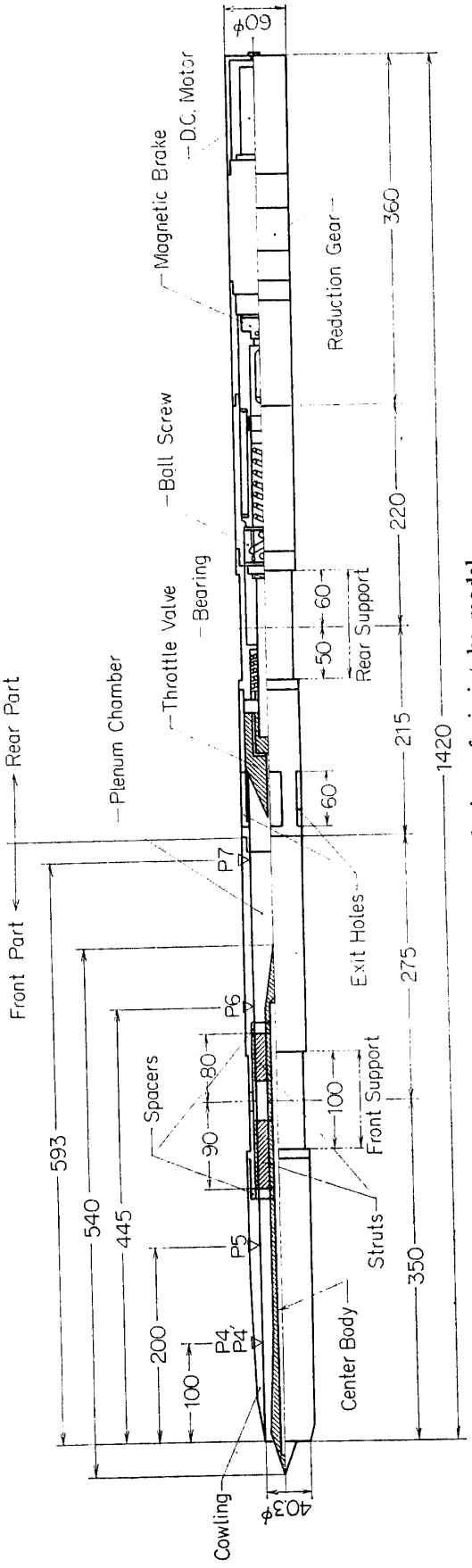

FIG. 9. General view of air intake model.

center body. As illustrated already in Fig. 8, therefore, the front end with pressure gauge holes is cut over its head like the windscreen of an airplane, for easy replacement of the broken gauge with a newer one.

The rear part: This part consists in a D.C. motor, a reduction gear, a micro magnetic brake, a ball screw and a slide register or a potentiometer. Thus the

TABLE 3. Spacer Combinations used for test.

Spacer Combination	Spacer thickness Front mm	Spacer thickness Rear mm	θ_A	A^*; Minimum Throat Area mm^2	T.R.($\equiv A_E/A^*$); Throttle Ratio	δ; Incidence of flow near cowling tip.
No. A	9.045	10.955	31°36′	540	0～2.41	$\delta=19°12'\simeq\delta_c(19°24')$
No. B	14.045	5.955	35°48′	609	0～2.14	$16°54'<\delta_c$
No. C	4.045	15.955	28°03′	484	0～2.69	$21°42'>\delta_c$

(θ_A; Inclination between centerbody apex and cowling tip.)

TABLE 4. Geometries of Cowling and Center Body in air intake model.

Cowling Outer Wall Geometry

$\tilde{x}$	$\tilde{y}$
0.0	19.268
6.76	24.00
20.00	27.00
120.00	30.00

Cowling Inner Wall Geometry

$\tilde{x}$	$\tilde{y}$
0.0	19.268
3.045	20.340
3.545	20.508
4.045	20.659
4.545	20.796
5.045	20.917
5.545	21.016
6.045	21.114
6.545	21.191
7.045	21.254
7.545	21.303
8.045	21.337
8.545	21.358
9.045	21.365
120.000	21.365
210.000	20.000

Center Body Geometry

x	y
0.0	0.0
30.000	13.989
30.050	14.215
31.000	14.428
31.500	14.627
32.000	14.813
32.500	14.986
33.000	15.147
33.500	15.296
34.000	15.433
34.500	15.558
35.000	15.672
35.500	15.774
36.000	15.866
36.500	15.946
37.000	16.015
37.500	16.074
38.000	16.122
38.500	16.159
39.000	16.185
39.500	16.201
40.000	16.206
40.927	16.188
240.000	8.384
250.000	8.000

conical throttle valve is drived to its to and fro movement by the electromotor, whose torque is increased through the reduction gear and converted through the ball screw with the least mechanical loss. The location of the throttle valve can be found out by the potentiometer, and is fixed to the desired position with the help of the magnetic brake. The area ratio between the inlet throat (A*) and outlet (A_E) is thus varied in the range of $A_E/A^*=0\sim2.5$, which is termed as throttle ratio.

As for the details about the geometrical profile of the center body and cowl lip, there is not so much difficulty to determine them, since an air intake of all external compression type is proposed. Two points to be cautious are that the normal shock never appears at the cowl lip in stable supercritical regime and that considerable loss should not occur in subsonic diffusion behind the throat. With these requirements, the cowling and the center body are designed whose detailed profiles are shown in Table 4, where ϕ_1 is restricted to 31°, δ_c is so designed by the conical field solution as to assure the smooth flow along the inner wall of the cowling, and the subsonic diffusing angle is everywhere within 7° avoiding too rapid area change causing into flow separation. The tip radius (R) of the cowl lip is 0.05 mm considering the structural and manufacturing requirements.

4.2 Model supporting system

The model used in the experiments is a very long one, because it contains at its duct end the throttle valve control system as shown in Fig. 9, and thus its total length reaches about 1420 mm.

Furthermore, it is desirable to change attack angle (α) for some range. Considering the requirement, the model is supported by two sets of strut or model supports. The front supporting strut is located downstream from the center of observation window as shown in Fig. 3. It is tried to reduce the strut thickness as far as possible without deficit in safety conditions. This strut is supported at both ends by ball bearings in order to endure the thrust suffered by the model and also to enable the rotation so easily in varying attack angle. The rear supporting strut (see Fig. 4) is located at the second throat block 500 mm appart from the front one and consists of two movable legs, which have a section of elliptic profile and are hinged to each shoe for clumping the rear part of model according to the change of attack angle. In this simple mechanism there will be no difficulty because of just a little shoe sliding on the surface of the model, even for the maximum attack angle ($\alpha=5°$).

5. Measurements

A schematic arrangement of the measuring system employed for the experiments is shown in Fig. 10.

The control history of static pressure in the settling chamber is taken by a strain gauge type pick-up and put into a pen or mirror oscillograph throughout the run of wind tunnel. Static pressure fluctuations at various model stations (P1~

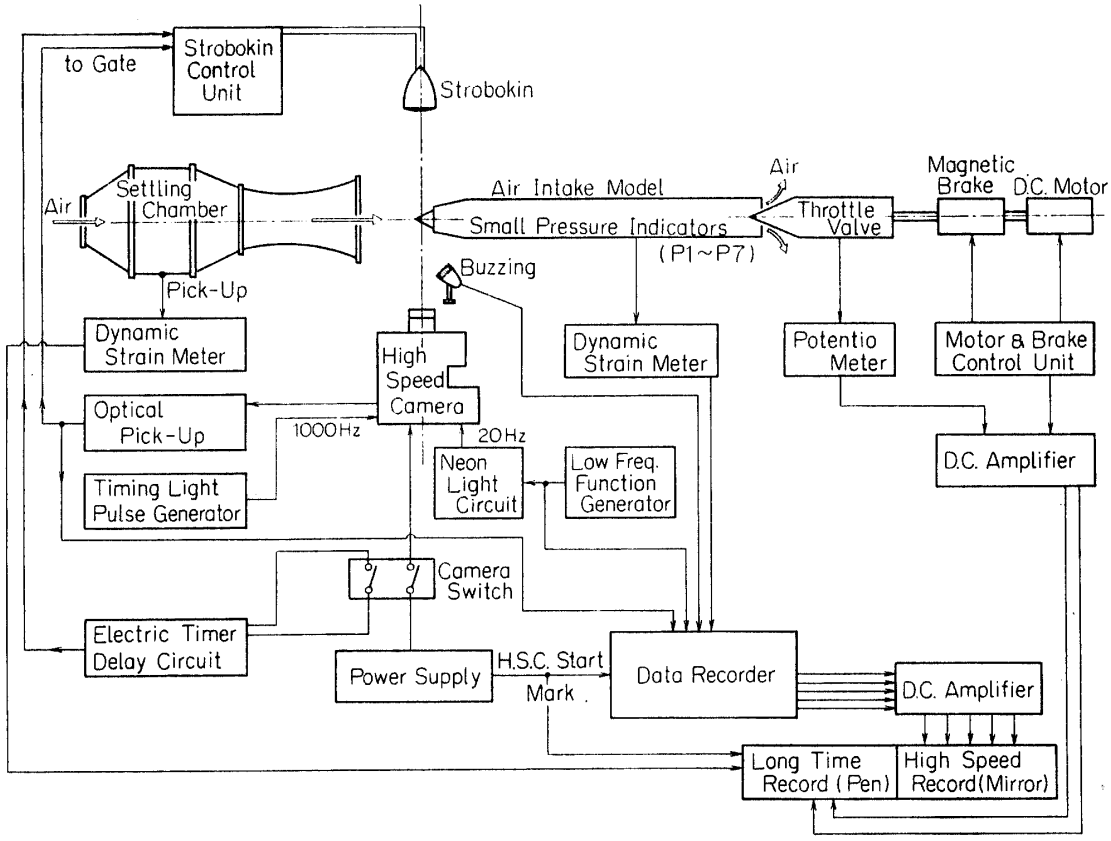

FIG. 10. Schematic arrangement of measuring system.

P7, see Fig. 8 & 9) are picked up by small pressure indicators equipped into the center body and the cowling wall. They are first recorded into a data recorder, synchronizing the operation of the movie films. Pressure indicators used in our tests are all strain gauge type with four gauges, and the pressure calibration curves are obtained by mercury manometer.

Schlieren photographic method is detailed in every literatures, so that we present here only the description about the light source and the high speed picture. The light source we can use is a high frequency flashing lamp, that is called "Strobokin" and produced by Impulsphysik Gmbh in German. Its intensity and possible flashing frequency are satisfactory up to some ten millisecondse for a high speed picture.

At the apex of the center body or near the cowl lip, oblique shock and expansion waves are recorded on either an ordinary monofilm or a 16-millimeter motion picture by using Strobokin as the light source for a Schlieren photograph. A high speed 16-millimeter movie camera, see Fig. 11, is controlled in its frame speed by input electric voltage, and the maximum is about 6000 frame per second. The start of Strobokin flashing is delayed by an electric timer about half of the film running time, and each flashing is synchronized to each frame of the movie in order to take pictures at an optimum flat region of the maximum frame speed, and also to indicate the correlation between the pressure records and the pictures.

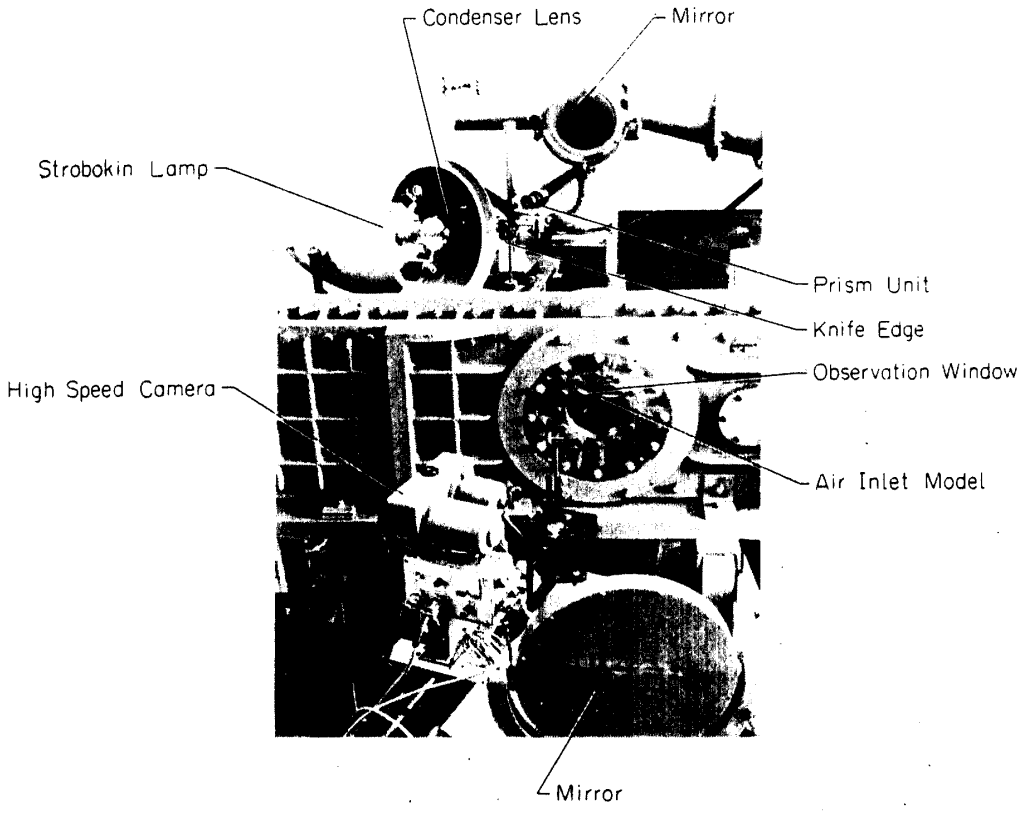

FIG. 11. Optical system for Schlieren method.

As synchronizing marks, 1000 Hz time mark and 20 Hz event mark are attached to both edges of the film and the latter mark is also transmitted to the high speed recorder passing through the data recorder. Camera starting signal and flashing impulses issuing from Strobokin are synchronized and put into the same data recorder.

The process of our experiment is as follows: First, all elements of measuring system are checked and the calibrated reference strain of each pressure gauge is recorded into the data recorder and long time recorder. Then the wind tunnel is started. After the control of the settling chamber pressure, a stable shock configuration of high supercritical regime is confirmed through the Schlieren photographic system, which shows regular supersonic flow in the tunnel test section.

Thereafter the throttle valve is controlled by D.C. motor and fixed at a certain position by the magnetic brake. The valve position is picked up by potentiometer, which is put into the pen-recorder or data recorder. At the same time, some panel photographs or a high speed movie are taken. After completing all cases for the throttle valve control, the operation of wind tunnel ceases and the measurements end. In this way experiments are performed for three cases of spacer combination, that is No. A, No. B and No. C, together with the cases of various attack angle.

6. Results and Consderation

6.1 Mean static pressure

In Fig. 12, the static pressure recovery $(P_{p.c.}/P_0)$ is plotted against the throttle ratio (A_E/A^*). As the throttle ratio decreases, the static pressure of the plenum chamber $(P_{p.c.})$ rises in a hyperbolic way. Up to the critical throttle ratio, that is 1.1~1.2, the flow configuration for each spacer combination is stable and no normal shock movement is observed.

Further decreasing the throttle ratio, the operation regime becomes subcritical and an unsteady pressure variation begins. Therefore the trend below this critical throttle ratio is based upon average readings of the manometer. The static pressure curve shows a peak at the critical throttle ratio and tends to descend for some range of succeeding throttle ratio decrease, which means the presence of a region of negative slope on the pressure recovery curve. Then it begins to rise again and reaches a certain value when the exit valve is completely shut.

Next the throttle valve is controlled reversely, that is, from completely shut condition to highly opened one. Although it intends to show hysterisis characteristics of buzz start and cease, there is no definite sign of this character with the exactness of our experiments.

As for the hyperbolic decrease of the plenum chamber pressure in supercritical regime, R. Hermann developed an explanation based upon one-dimensional continuity equation [*11*]. In our case exit nozzle holes locate at the side wall of the outer cyliner (or the cowling), so that the deviation of experimental data from Hermann's explanation, in particular for spacer No. B in higher throttle ratio, is likely to be caused by three dimensional effects.

Distributions of the static wall pressure measured along the axis of the air intake are illustrated in Figs. 13a~c, where the experimental results are compared

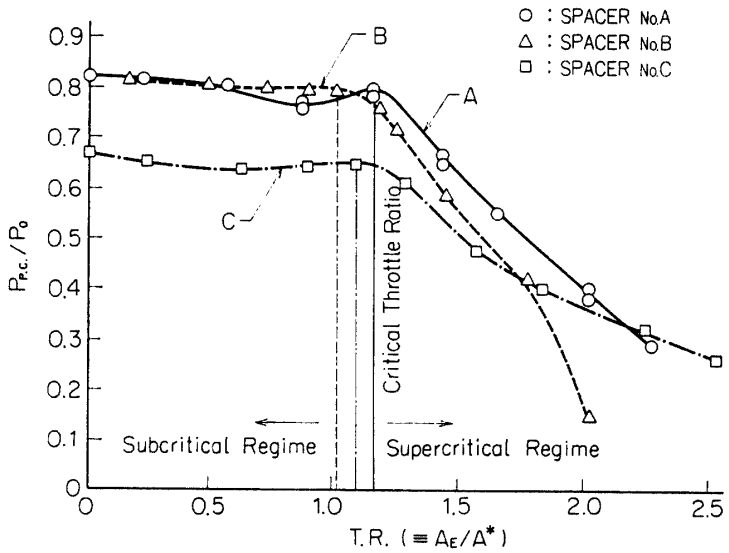

FIG. 12. Comparison of static pressure recovery.

with the values calculated assuming one-dimensional isentropic compression. These static pressure are obtained by the traces of pressure indicator operation at six stations which are located at important positions, such as the cone surface (P1~P2), the throat (P3), the diffuser before the front strut (P4 & P5), the diffuser after the strut (P6) and the plenum chamber (P7). As shown in these figures, the static pressure steadily increases with the decrease of the throttle ratio. Below the critical throttle ratio (marked by * in Fig. 13), buzz begins.

Static pressure distributions with the flow feature near the cowl lip are also detailed in Figs. 14a~c, in which there are both lines of static pressure and Mach number calculated by one-dimensional flow theory with the help of a conical field table and Prandtl-Meyer expansion theory, assuming the shock configuration for

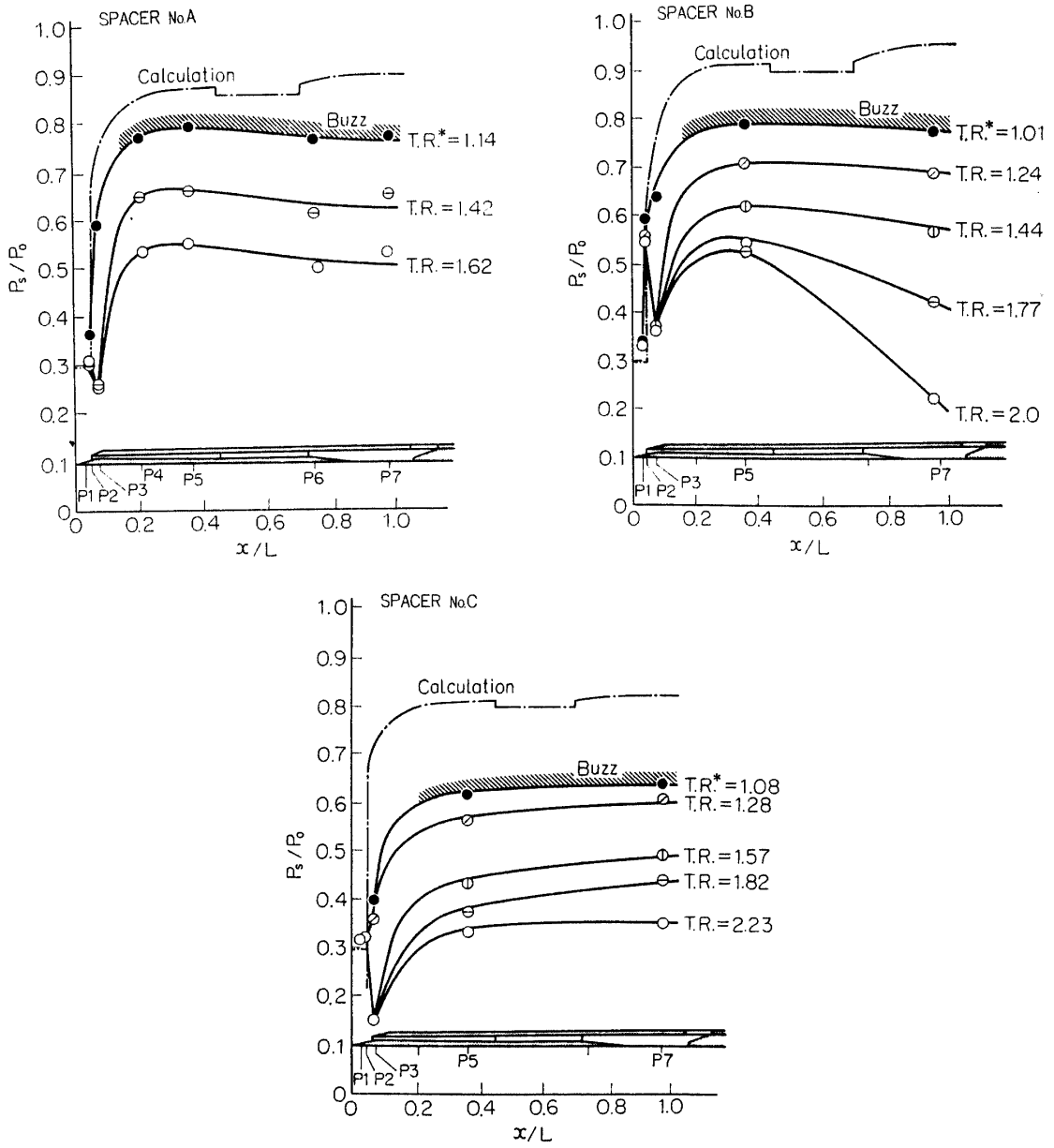

FIG. 13. Distribution of static pressure along model axis.

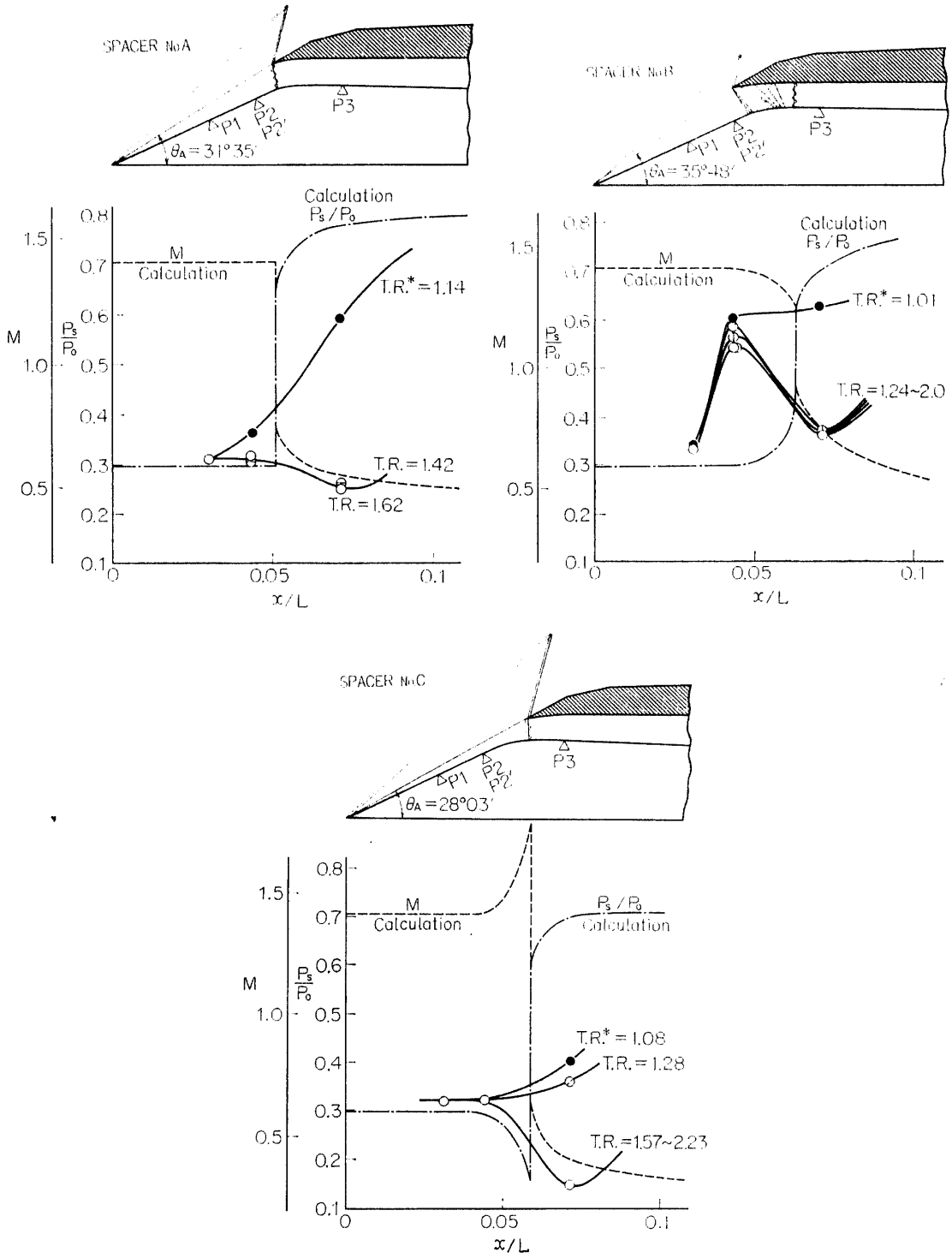

FIG. 14. Distribution of static pressure near cowl lip.

each spacer combination. Both pressure distributions near the cowl lip for Spacer No. A and No. C are very similar as shown in Fig. 14, but showing the extreme difference from that measured for Spacer No. B, where the inclination $\theta_A(=35°48')$ is a little or more larger than the inclinations for No. A ($=31°36'$) and No. C ($=28°03'$).

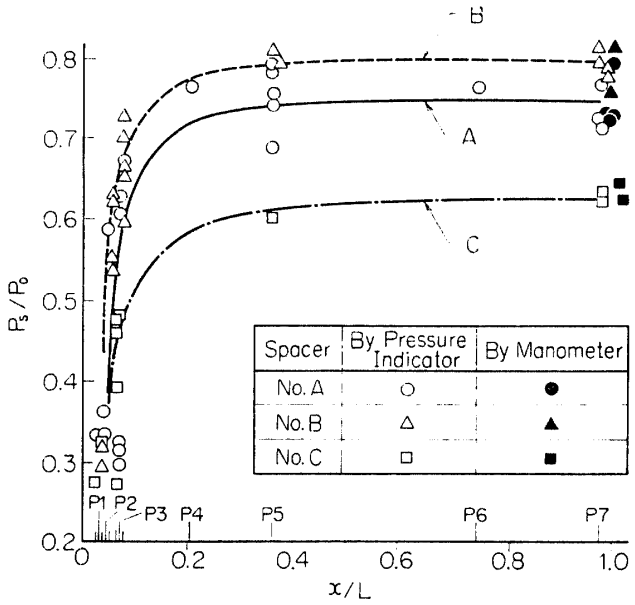

FIG. 15. Static pressure just before buzz start.

The static pressure just before buzz start are plotted for each spacer combination in Fig. 15, where the values of P7 are compared to the direct readings of a mercury manometer, which are shown by black marks. These results show the reliability of pressure indicators of strain gauge type. The scatter of measured static pressure is possibly due to the effects of sudden temperature drop in supersonic air flow and some mechanical restriction in setting the pressure indicators.

In the supercritical regime with higher throttle ratio than the critical one, static pressure at the plenum chamber steadily increases with the decrease of the throttle ratio and there is no evident pressure jump due to normal shock but gradual pressure increase behind the throat. Then supersonic flow is established even behind the throat at such a high supercritical regime, in which bow shock attaches at the cowl lip. Such stable shock configurations for each spacer combination are compared with unstable ones during the so-called inlet buzz in Fig. 16.

6.2 Characteristics of inlet buzz

As decreasing further the throttle ratio, the non-stationary flow phenomenon occurs in the supersonic air intake of external compression type. The static pressure fluctuation recordings by the pressure indicators installed in the model are shown in Figs. 17, being the throttle ratio as a parameter over the complete range of operation. Time and pressure scale are indicated to each recording. There is no obvious pattern change through all three spacer combinations, except for low throttle ratio range of Spacer No. C.

At highly supercritical operation all pressure indicators show perfectly stable flow. Only P5 and P7 fluctuate slightly with random high frequency, which might be caused by flow separation in subsonic diffuser behind the minimum throat. Near the critical point unstable features come into activity. In most cases, the

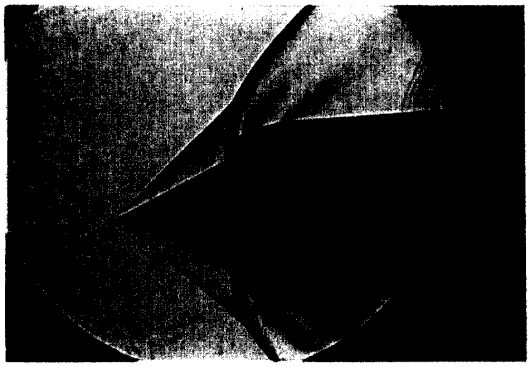

SPACER No.A
T.R. = 1.42

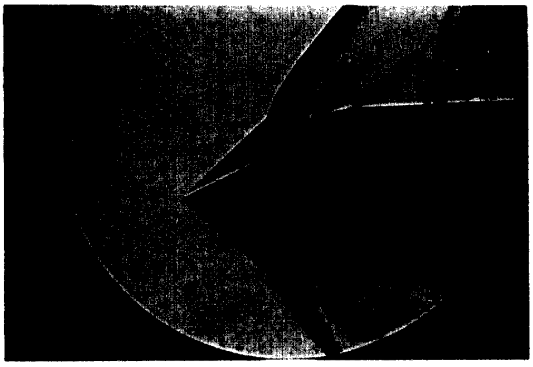

SPACER No.A
T.R. = 0.55

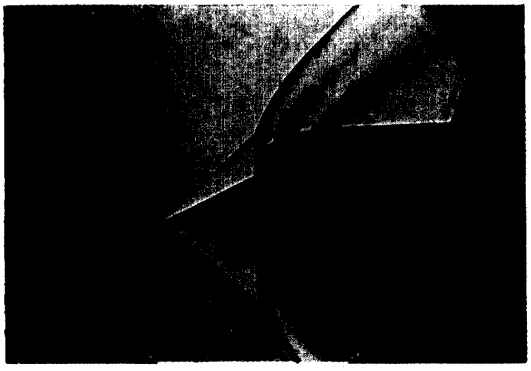

SPACER No.B
T.R. = 1.24

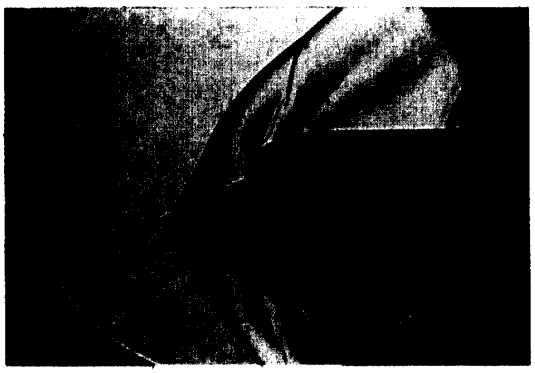

SPACER No.B
T.R. = 0.49

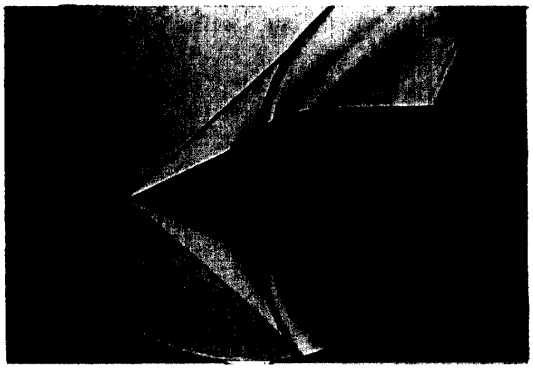

SPACER No.C
T.R. = 1.82

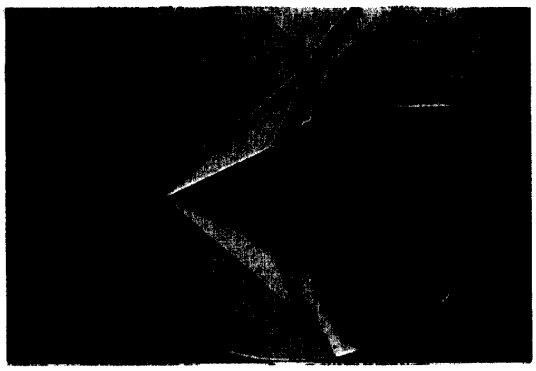

SPACER No.C
T.R. = 0.60

Supercritical regime
(Stable)

Subcritical regime
(Unstable)

FIG. 16. Typical shock configurations at supercritical and subcritical regimes.

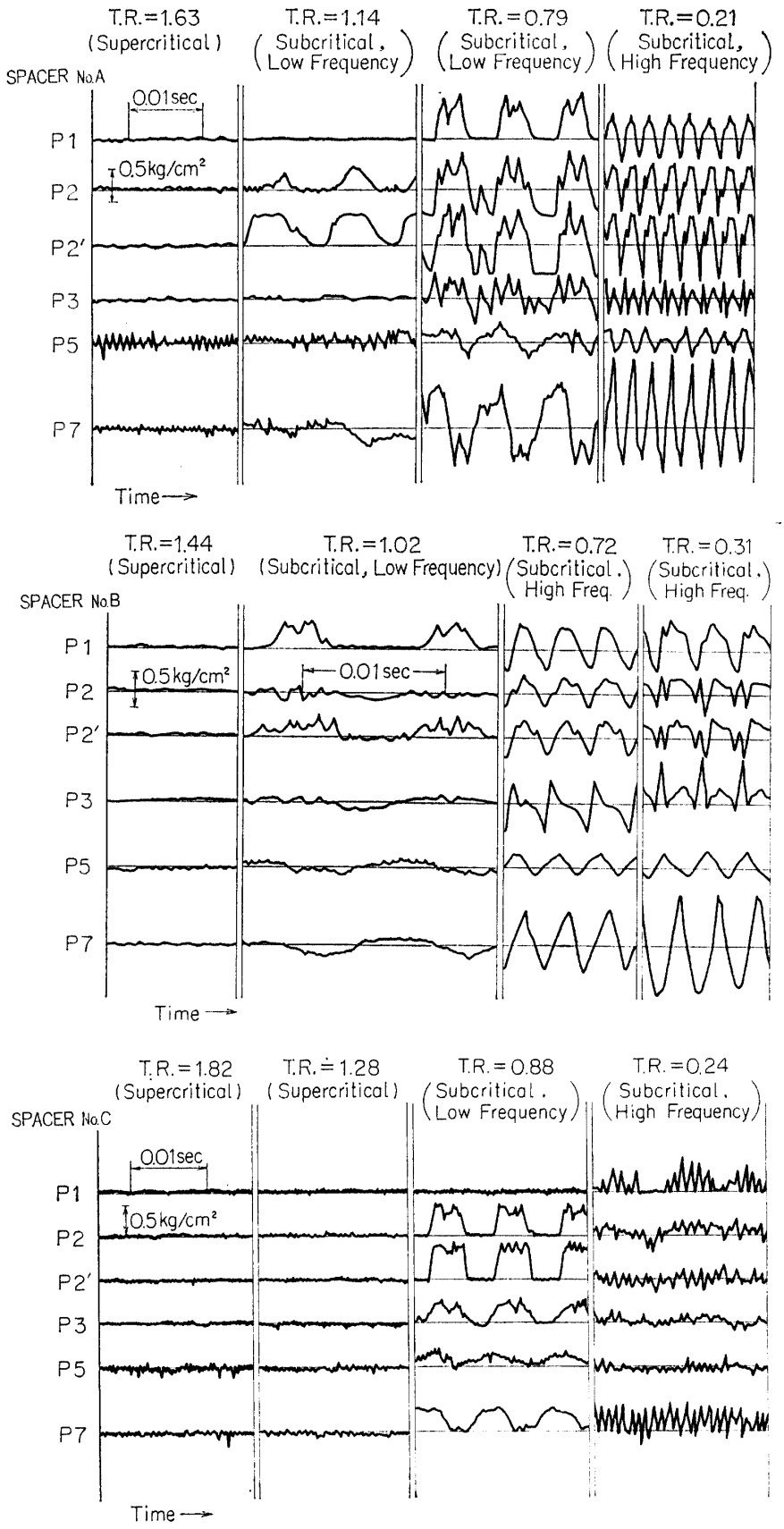

FIG. 17. Pressure fluction for each throttle ratio.

first sign of these appears in pressure pick-ups equipped close to the cowl lip, that is P2 and P2′ for Spacer No. A and P1 for Spacer No. B.

As we see from Fig. 17, there appears in every pressure indicator, a series of random up-impulse of not very large amplitude for each spacer combination. These impulses, however, are predominant in vain, until unstable tendency comes up to the rear stations of P5 or P7. In this stage, oscillation hardly prevails and the occasional radom impulse seems to have little effect on the plenum chamber (P6 or P7).

After transition when buzz cycle is completely established, pick-ups, P2 and P2′, show step-like pressure variation, although P5 and P7 do a more sinsoidal oscillation. At the bottom part of this step-like fluctuation pattern the flow is stable, while the upper part is composed of certain high mode oscillation. This might indicate the presence of rather complicated disturbance during the shock being expelled as illustrated in the unstable regime of Fig. 16. The repetition of buzz cycle is not exactly complete one. The average fluctuation in pressure recording of P3 shows the most arbitrary manner in amplitude, while P5 has rather small amplitude compared to the other pick-ups.

In detail to examine such transient processes as the first occurrance of cyclic

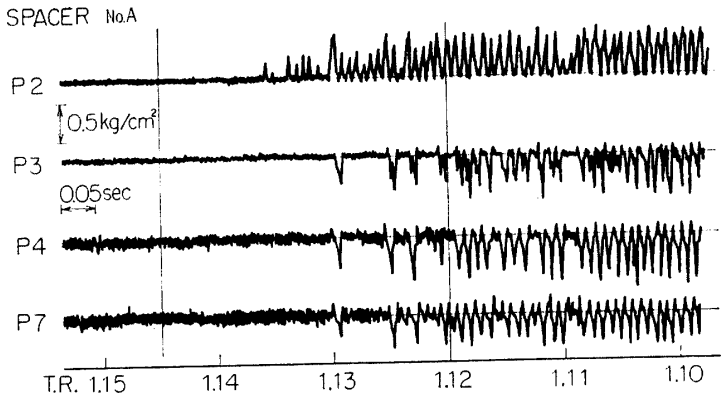

FIG. 18. Occurrance of inlet buzz with low frequency, according to decrease in throttle ratio (1.18→0.97).

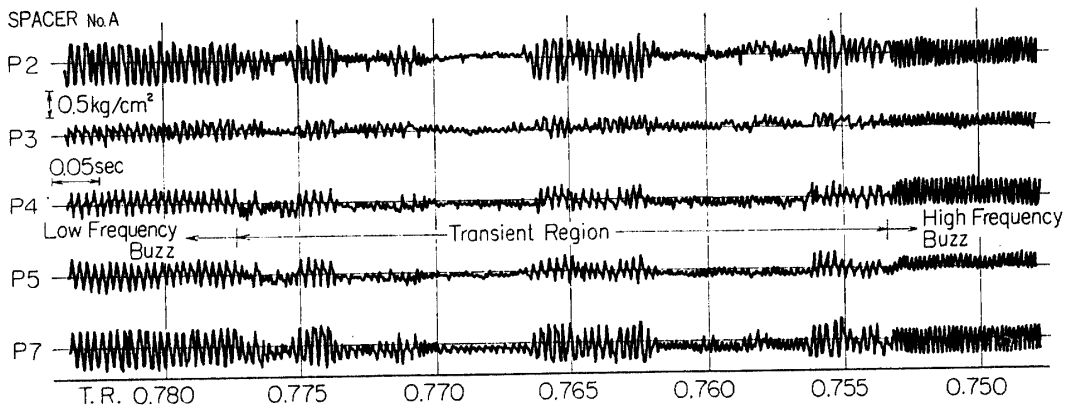

FIG. 19. Transient process from Low Buzz to High Buzz.

pressure fluctuation and the transition from low frequency buzz to high frequency one, we control the throttle valve very gradually, putting the pressure variations at every stations into the data recorder.

For Spacer No. A, the occurrance of inlet buzz with low frequency from the stable supercritical state is shown in the pressure recording of Fig. 18. The initial

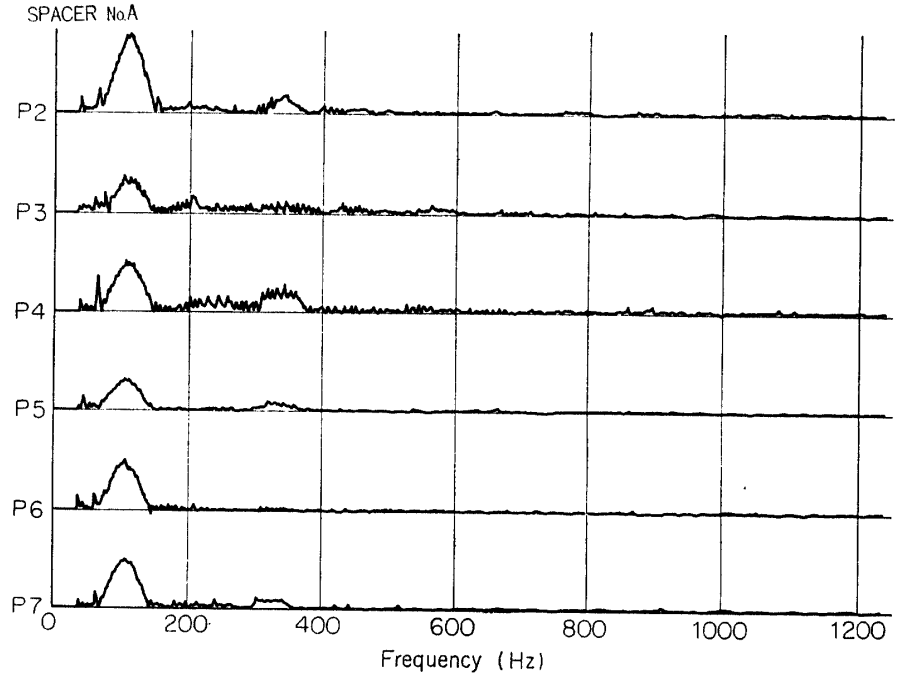

a) Low Buzz (T.R.=0.97)

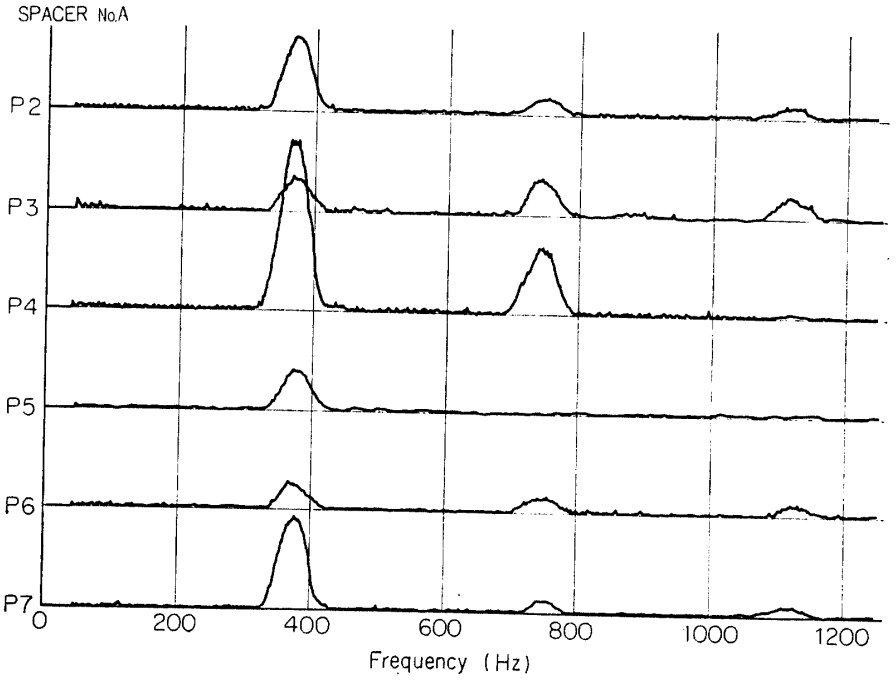

b) High Buzz (T.R.=0.55)

FIG. 20. Frequency analysis of pressure fluctuation.

pulse appears at the cone surface of the center body (P2), and then a little larger pulse of P2 follows suddenly at the other stations (P3~P7) after some delay from the first pulse.

Further decrease of the throttle ratio brings a drastic second transition. This second phase of buzz, which we name high frequency buzz, prevails until the throttle valve is finally shut, and is characterized by higher frequency about 3 or 9 times of the first buzz frequency and comparable or much larger amplitude of pressure oscillation. As shown in Fig. 19, during the transition from low frequency buzz to high frequency one, there are a few ceased regions in spite of decreasing the throttle ratio continuously. It is very important to emphasize that there is almost no phase difference between every pressure variations during this transient process.

These pressure recordings, e.g. Fig. 17 & 19, are examined in frequency with the aid of Power Spectrum Analyser of Noise Frequency. The characteristic frequency for Spacer No. A is shown in Fig. 20, in which some peaks are possible

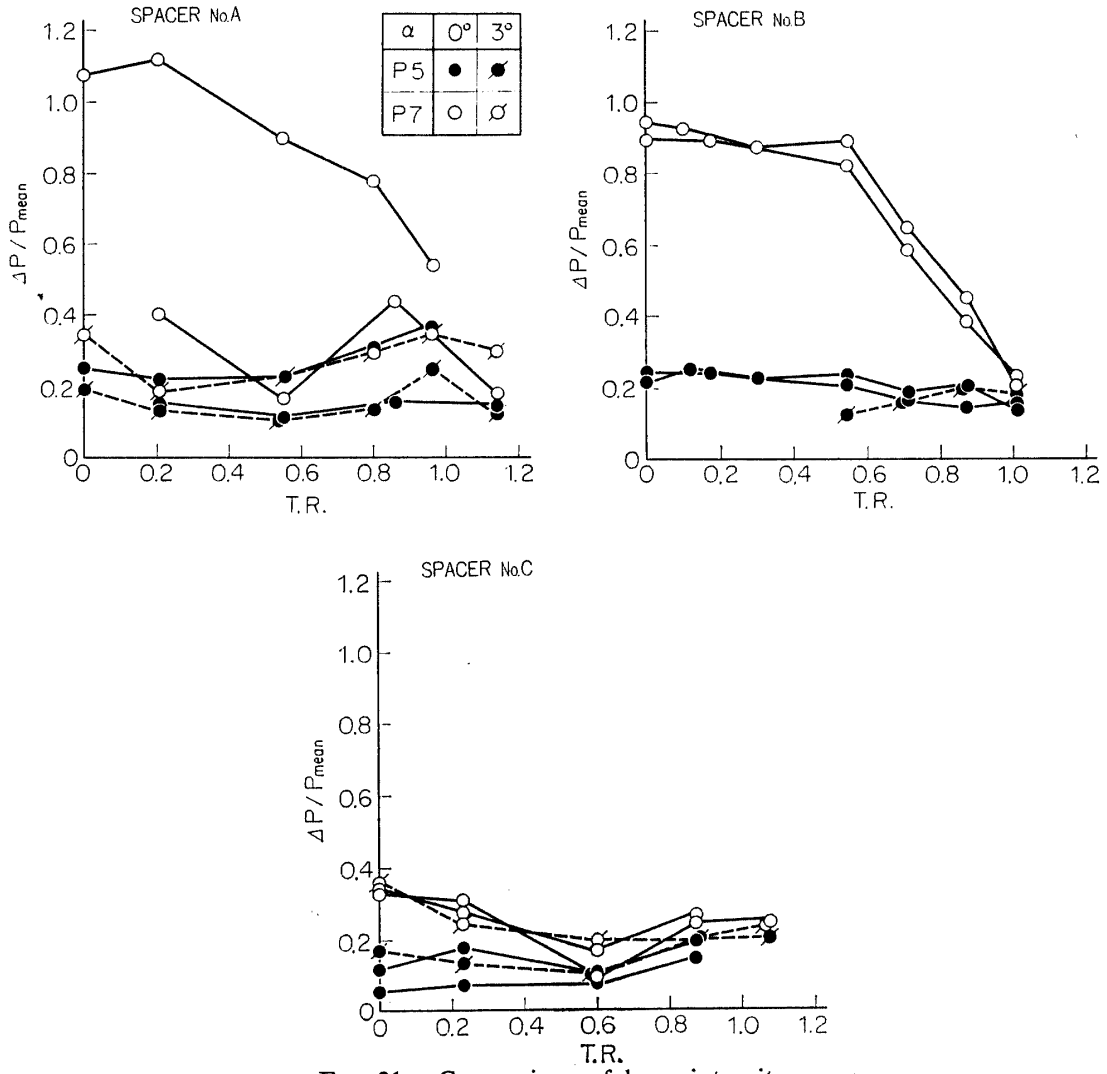

FIG. 21. Comparison of buzz intensity.

to become intense. During the first unstable region, the peak of near 100 Hz becomes predominant commonly to all pressure pick-ups, so that the unstationary flow in this region is called as the inlet buzz with low frequency or for short Low Buzz. This predominant frequency does not prevail so long if we further decrease throttle ratio. Thus, in High Buzz appear also higher order frequencies than the low frequency, coexisting with the predominant one, as may be seen from Fig. 20. The reason is not yet clear why a certain frequency becomes predominant among them and why High Buzz has several frequencies of nearly three, six or nine times the predominant frequency in Low Buzz.

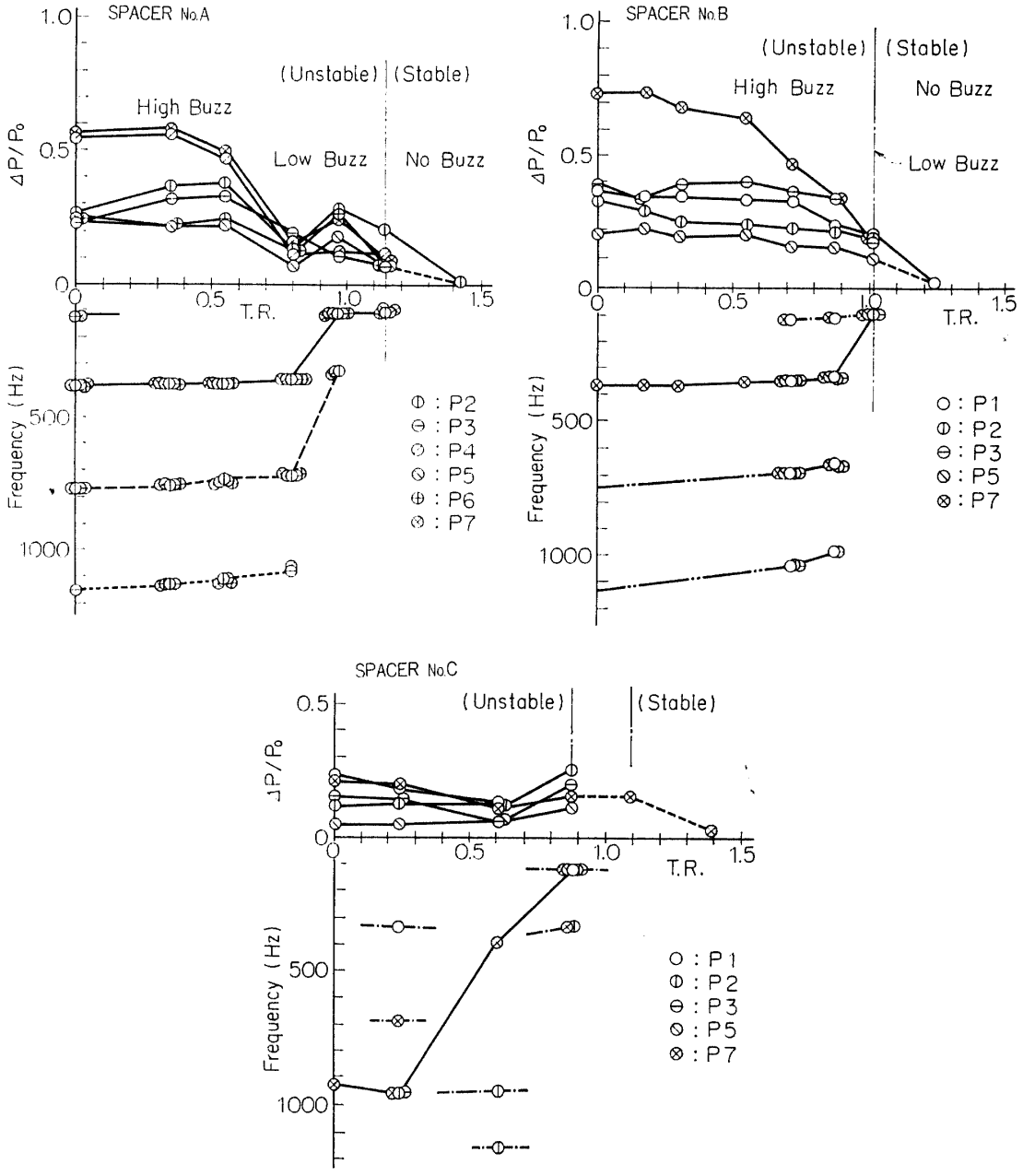

FIG. 22. Comparison of pressure fluctuation and buzz frequency ($\alpha=0°$).

Corresponding amplitudes of such pressure fluctuation, that is named buzz intensity, show rather arbitrary behavior as shown in Figs. 21a~c. At the start of inlet buzz the amplitude relative to the time mean pressure (P_{mean}) is below about 0.3 and it indicates larger value at the rear pressure indicator (P7) than at the front (P5). As the throttle ratio decreases it tends to rise up again for Spacer No. A & B. On the other hand, the considerable decrease of amplitude is seen in Spacer No. C including the vivid tendency of cease at T.R.=0.6 during the second transition.

Both the amplitude and the frequency of pressure fluctuation for each spacer combination are plotted against the throttle ratio in Figs. 22, where the above explanation is proved. Thus from the figures, they are summarized as follows:

1) There are some characteristic frequencies, one of which becomes predominant according to the throttle ratio. 2) Two or three characteristic frequencies are coexisting over the both buzz regimes, including the transition from Low Buzz to High Buzz. 3) The amplitude of pressure fluctuation or buzz intensity shows rather arbitrary manner. 4) According to the throttle ratio control, there occurs an oscillation of weak pressure fluctuation at P7 for Spacer No. C, while stronger fluctuation happens for the other spacer combinations.

6.3 Movie analysis

To examine the detailed features of the cyclic phenomenon, Inlet Buzz, the bow shock traveling along the center body surface is photographed by a high speed camera using Storobokin lamp as a light source. And also corresponding pressure recordings are obtained together with the frequency spectrum. Here we treat the only case of Spacer No. A. The frames of movie films are numbered on the left in order to correspond to the numbers on the top of the pressure recordings.

Figs. 23 show the shock movement and the pressure fluctuation for the throttle ratio=0.97, that is Low Buzz regime. Camera speed is about 5600 frames per second. As shown in Fig. 23a, at Frame No. 41 the normal shock wave is just ahead of the cowling and then rapidly reaches to a certain farmost position from the cowl lip and stays in the range of Frame No. 53~64. The traveling feature of the shock wave shows somehow unsymmetrical manner, which might be due to a slight eccentricity in the location of the center body. Up to Frame No. 73 or 74 the expelled shock is completely swallowed, (c.f. succeeding 16 frames show that the shock is staying within the cowl lip) and thus a cyclic traveling of shock wave is to be completed with so-called low frequency of about 100 Hz.

In Fig. 23b, such a shock movement is compared with the pressure fluctuations at the several stations of the model (P2~P7). The pressure variations at P2 and P3 exactly respond to the shock motion during which it rises from the bottom to the top of pressure record in steplike manner to time, where it keeps its value for some succeeding frames. Relating to P2, higher mode oscillations come into sight on the top plateau which continues about 20 frames. These higher order fluctuations can be also found in the bow shock movement. If you examine the photographs carefully, you can remark the tangent of the bow shock leg oscil-

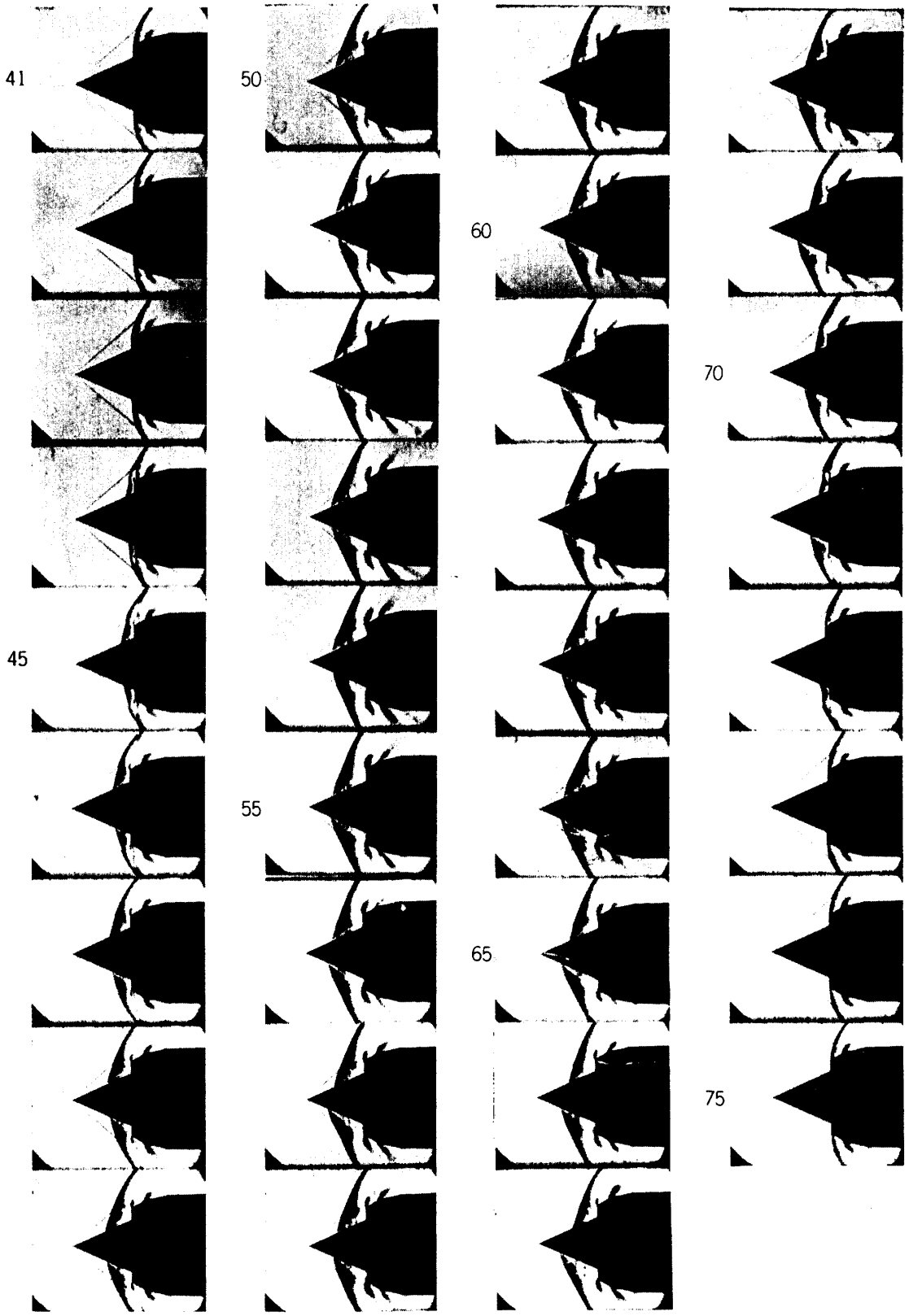

FIG. 23. a) High speed photographs of shock traveling during Low Buzz regime. (Spacer No. A, T.R.=0.97, frame speed 5600 F/S).

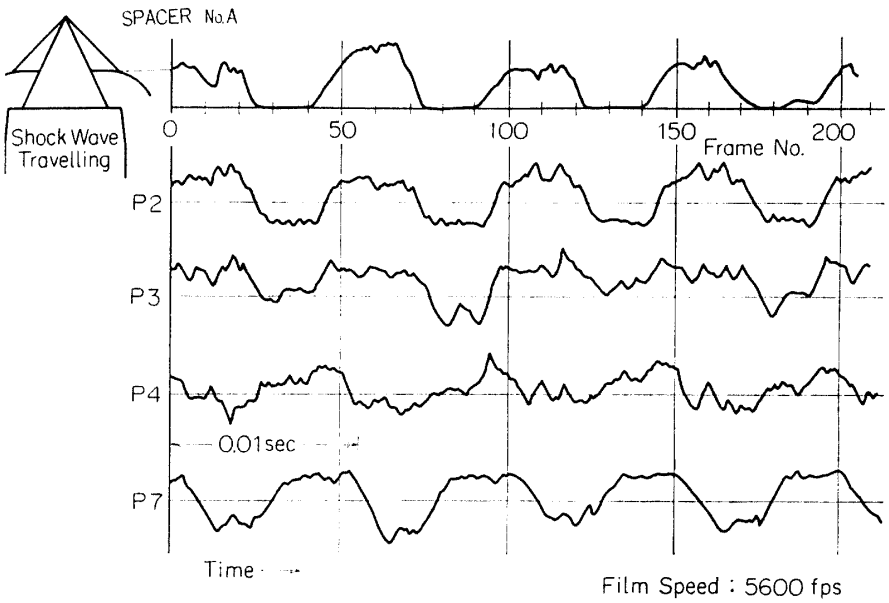

FIG. 23. b) Correlation between shock traveling and pressure fluctuation during Low Buzz regime (T.R.=0.97).

lates near the cone surface. Then boundary layer separation may be the cause to discern such characteristics. Now fluctuating pressure near the cowl lip is on its way to descend corresponding to the shock movement. However P4 behaves in rather complex manner, more sinusoidaly than step-like. The static pressure in plenum chamber (P7) varies step-like manner as well as that at P2, but with considerable advance of about 15 frames as indicated in Fig. 23b.

The second example is to the throttle ratio=0.67 for High Buzz, and illustrated in Figs. 24a~b. Camera speed is 5800 frames per second. From the photographs in succession, the normal shock is attached at Frame No. 22 and at Frame No. 27 the shock just reaches to the far-off position from the cowl lip, and then it is swallowed into the cowling near Frame No. 37. Thus the cycle of shock movement is repeated with a high frequency of about 360 Hz. The shock traveling shows also a good correspondence to the pressure fluctuations at P2~P7, although there is some delay time between them. In the pressure recordings, the shock wave pattern becomes more sinusoidal and gives no vivid sign of movement in step-like manner, so that the shock wave is considered to be always in motion. The pressure patterns at P2 & 3 are somehow disturbed by higher harmonics, frequencies of which are about 360, 720 and 1080 according to the analysis by using the Spectrum Analyser. On the contrary, the pressure fluctuation in the plenum chamber, P7, is quite similar to the shock movement pattern, as well as in the case of Low Buzz, although there is more or less phase difference between them.

For other spacer combinations we can briefly say that there seems no drastic change of pattern in the shock movement and the pressure fluctuation. As referred to Spacer No. C, however, the pressure record corresponding to the predominant frequency has no established wave pattern, although the characteristic frequency

can be picked up in every pressure indicators except for P1. This station is located too far from the cowl lip to give any sign of oscillation. After complete transition into High Buzz, as shown in Fig. 17c, P1 oscillates fiercely as comparable with P7, while the other indicators remain to do not so heavily but in random manner. The bow shock wave ahead of the cowl lip does not change its position greatly,

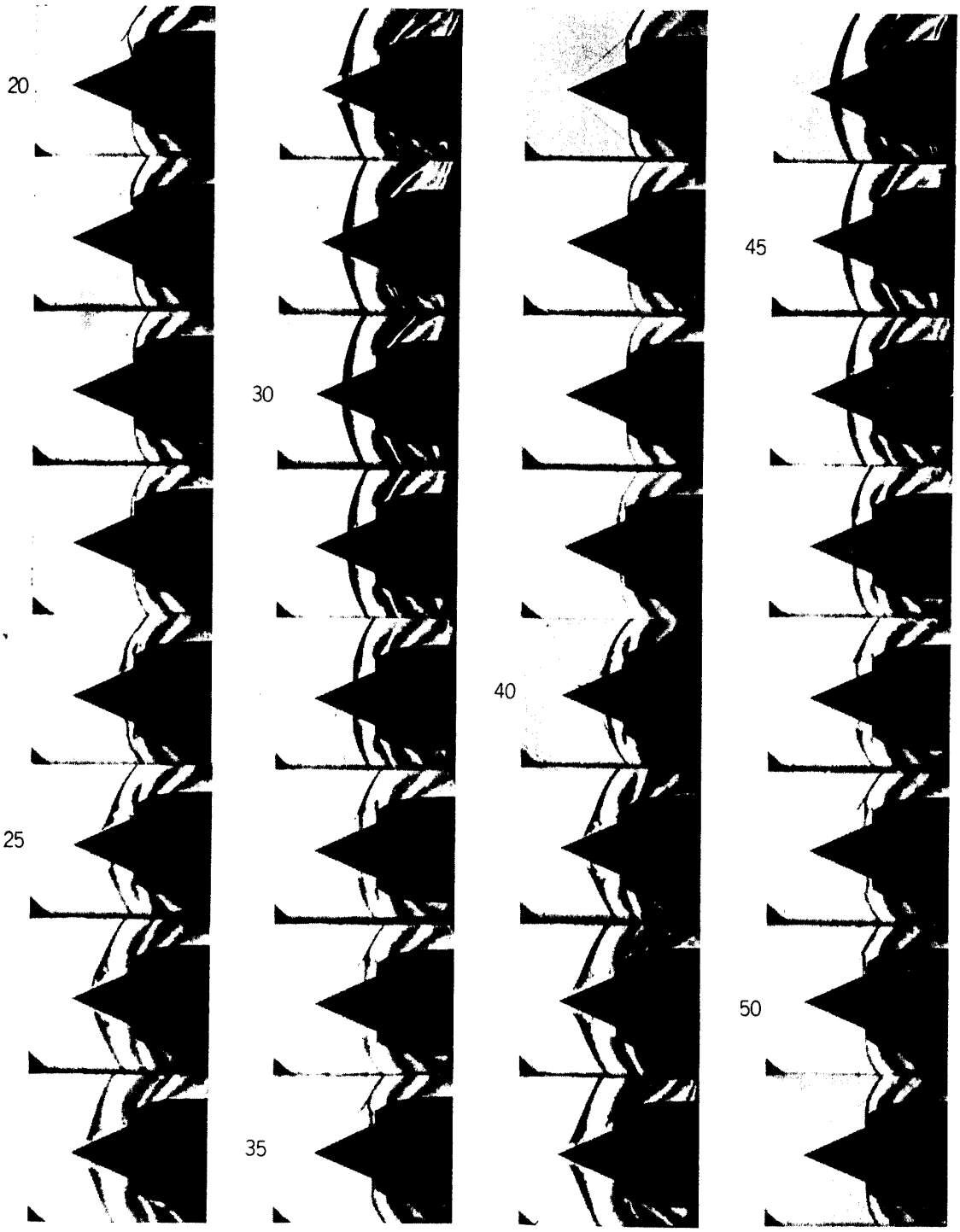

FIG. 24. a) High speed photographs of shock traveling during High Buzz regime. (Spacer No. A, T.R.=0.67, frame speed 5800 F/S).

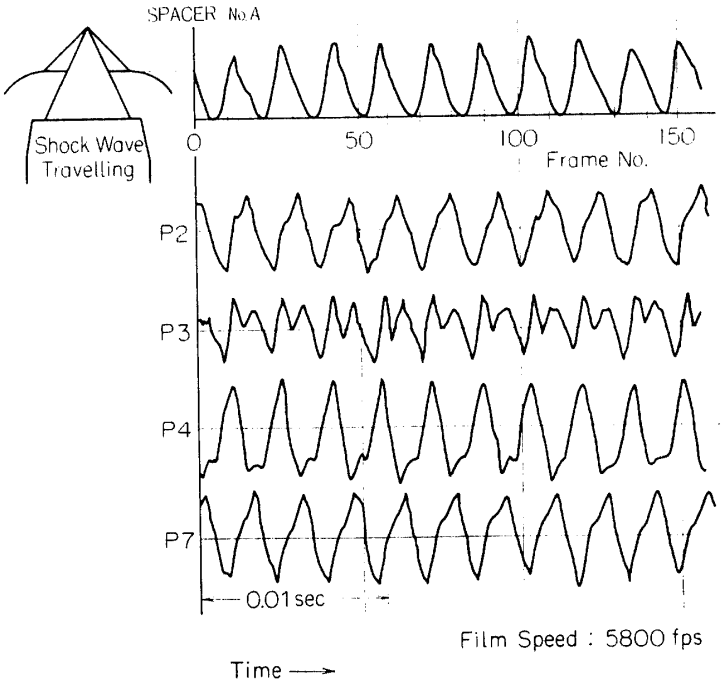

FIG. 24. b) Correlation between shock traveling and pressure fluctuation during High Buzz regime (T.R.=0.67).

but experiences a small oscillation.

In these courses of observation, we obtain: 1) The motion of the bow shock wave corresponds fairly well to the pressure fluctuations measured at several stations of the model. 2) The power spectrum analysis for the pressure fluctuations indicates the presence of higher order components, besides the predominant one which governs all pressure fluctuations at a certain throttle ratio. 3) For Spacer No. C the predominant frequency changes very much towards higher order according to the decrease of throttle ratio.

Finally, the effect of attack angle to each spacer combination is examined according to the above procedure for non-attacked cases, where attack angle is varied to 3° or 5°. All but one experimental results are omitted here. Because there is no obvious effect of attack angle on the throttle ratio at buzz start, and buzz frequency is also not affected much by attack angle. The flow features in attacked cases, however, show vivid unsymmetrical manner in which the windward bow shock on the center body is expelled out from the cowl lip. Behind this shock wave a wide separated region is observed, which may be responsible for the superposed small fluctuation on the pressure recordings of P2.

As the only results in attacked cases, buzz intensities for each spacer combination are compared with those measured for non-attacked cases in Figs. 21. There is also no large effect of attack angle on the buzz intensity, as we presumed.

6.4 Consideration about inlet buzz

In Fig. 25, the pressure fluctuations at every stations (P2~P7) are shown for two representative throttle ratios of both Low Buzz and High Buzz. From these

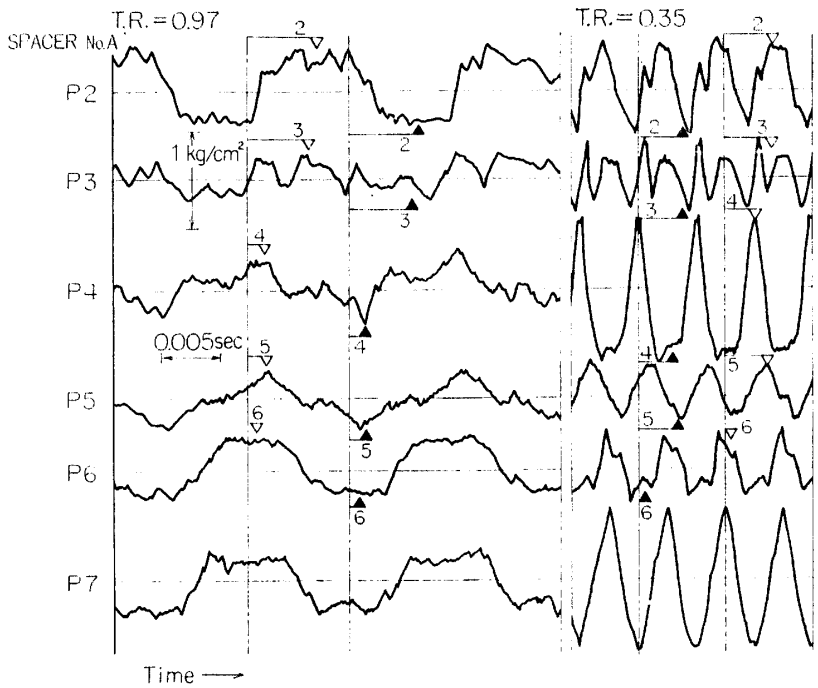

FIG. 25. Pressure fluctuation in inlent buzz.

data, the amplitude ratio ($\Delta P/\Delta P7$) and the phase relation ($\phi_{\Delta P}$) can be plotted versus longitudinal stations schematically show at the bottom of Fig. 26. These results are all referred to the station of P7. In addition, there is also plotted the case where the experiments are made without the center body and with completely shut exit nozzle (T.R.=0.0). The result for the case without the center body has a good tendency in its amplitude ratio distribution towards the entrance which can be proved by a simple acoustic resonance tube theory. Frequency, calculated as $f \cong 130$ Hz, is also coincidence with the measured frequency ($f=$ 140 Hz) for this case.

The actual distribution of the amplitude ratio during buzz varies in rather arbitrary way along the model axis depending upon the throttle ratio, so that we cannot draw out any opinion about the amplitude ratio. On the other hand, the comparison in phase relation shows better agreement between Low Buzz and a simple acoustic model with a nodal point near the rear exit. The data points for Low Buzz are close to those of the case without the center body and both of them show almost the same phase along the model axis behind the entrance. The frequency is also in good agreement, as you see from the table in Fig. 26. Thus the phenomenon of Low Buzz if viewed from a traveling wave system, seems to behave like a standing wave.

For High buzz, the data points become scattered in the phase distribution as well as the amplitude distribution. If we estimate the mode of oscillation, on the analogy of Low buzz case, from the fact that High buzz has the frequency 3~4 times of Low buzz, we say that there is another nodal point inside the duct and the phase is changed by π at that point. Then we guess from Fig. 26 that

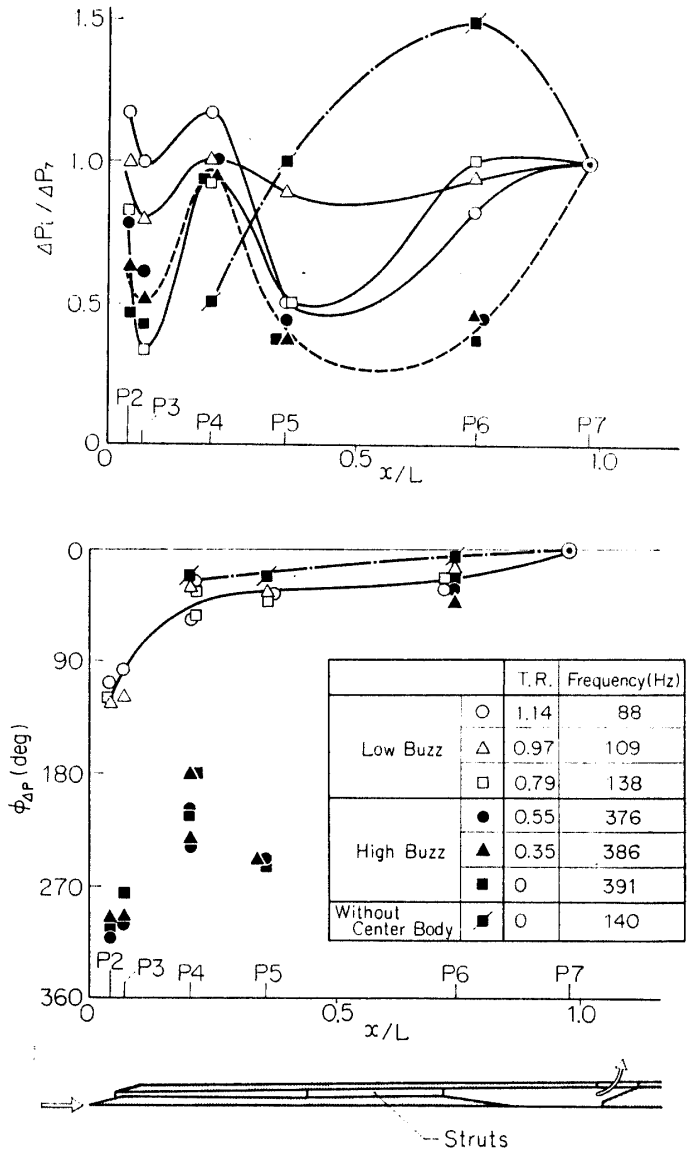

FIG. 26. Amplitude ratio and phase relation of fluctuating pressure.

the nodal point is located between P5~P6. We can also notice that the data points at P4 and P5 look about the same phase lag against P6 and P7. However, the actual value of phase lag is more than π. Another difficulty is how to explain the phase lag by $\pi/2$ between $P2$ (or $P3$) and $P4$ (or $P5$) that happenes for both cases of Low and High Buzz, where the presence of shock wave may play a part.

These deviations from a simple accoustic model might be due to the mass flow through the model, the area variation along the model axis including blockage effect of strut and the boundary conditions at the entrance and the exit. In particular, we should notice that the entrance condition may differ largely according to whether the center body is inserted in the air intake or not.

It is also difficult to get any idea to explain the shift from Low Buzz to High Buzz. Only one point we can say is that in our experiments without the center

body we could not get oscillation of about the same order frequency as High Buzz, so that the presence of center body may play an important role in this transition.

7. Conclusion

Inlet buzz starts only when the throttle ratio decreases below the critical point and before the buzz starts random pressure pulses at the front part of air intake cause no response at the plenum chamber. These facts suggest that the pressure level at the rear part plays inherent role upon the instability of supersonic air intake. Thus it will be proposed to stress the distinction between the origin leading to instability and the inherent character of the inlet system, where the entrance and exit conditions should be further discussed.

Now we finally summarize the results of our experiments of inlet buzz as follows:

1) In the supercritical regime there is no pressure fluctuation at every stations of air intake model and a bow shock is attached ahead the cowl lip.

2) Near the critical point unstable feature comes into activity. In the sub-critical regime we observe occurrence of nonstational phenomena, named as Inlet Buzz, which include cyclic pressure fluctuations and shock wave traveling.

3) Inlet buzz has two characteristic frequencies, one is about 100 Hz and the other three times of that value, together with further high harmonics.

4) The transition from lower frequency to higher one happens according to the decrease of the throttle ratio, while the amplitude of pressure is fluctuated in rather arbitrary manner.

5) The motion of the bow shock wave corresponds fairly well to the step-like pressure fluctuation at the front part of the model. Schlieren photographs show complicated behaviour of the boundary layer on the center body surface when it is expelled out from the cowl lip.

6) As for the frequency of these cyclic phenomena, both frequency bands, low and high, measured by using Spectrum Analyser coincide qualitatively with those calculated under the assumption of a simple acoustic model.

7) For spacer combination, there seems no drastic change of pattern in the shock movement and the pressure fluctuation, excepting only the case of Spacer No. C, where the predominant frequency changes very much toward higher order as decreasing the throttle ratio.

8) No obvious effect of attack angle is found on the throttle ratio at buzz start, the buzz frequency and the buzz intensity. The flow features in attacked cases, however, show vivid unsymmetrical manner and a wide separated region behind the shock wave.

Acknowledgements

The authors wish to thank to Mr. Tanikatsu for his continuous assistance in the course of the experiments, and to Associate Prof. Tanida, Dr. Okajima and Dr. Kaji for their valuable suggestion on this study. As for the supersonic wind

tunnel test, great deal of information and experimental instruments are offered by Mr. Seki to whom we really express our thanks. Also we are indebted to Mr. Kubota and Mr. Amino for their help concerning the wind tunnel operation.

Department of Jet Propulsion
Institute of Space and Aeronautical Science
University of Tokyo, Tokyo
May 10, 1972

References

[1] Kl. Oswatisch, NACA T.M. 1140 (1947).
[2] A. Ferri & L. M. Nucci, NACA REP. 1189 (1954).
[3] A. Kantrowitz, NACA W.R. L-713 (1945).
[4] A. Kantrowitz, NACA T.N. 1225 (1947).
[5] A. Ferri & L. M. Nucci, NACA R.M. L50K30 (1951).
[6] C. L. Dialy, J. Aero. Scie. 22-11, (1955), 733.
[7] W. H. Sterbentz & J. C. Evvard, NACA T.N. 3506 (1955).
[8] W. H. Sterbentz & J. Davids, NACA T.N. 3572 (1955).
[9] R. L. Trimpi, NACA T.N. 3695 (1956).
[10] R. L. Trimpi, NACA REP. 1265 (1956).
[11] R. Hermann, Minneapolis Honeywell Regulator Co. (1956).
[12] R. Kawamura, & el., Bulletin of Aeronautical Research Inst., Univ. of Tokyo 3-6 (B) (1963).
[13] M. Namba, T. Asanuma, Report of Institute of Space and Aeronautical Science, Univ. of Tokyo 1-3 (B) (1965), 164.
[14] M. Tucker, NACA T.N. 2045 (1950) and 2337 (1951).
[15] О. М. Белочерковский, Обтекание Затуленных Тел Сверхзвуковым Потоком Газа (В. Ц. АН СССР)

Notations

A_E	exit area
A^*	minimum throat area
a	sonic velocity
D	outer diameter of air intake model
D_C	inner diameter of plenum chamber
D_i	diameter of cowl lip
d	maximum diameter of center body
L	length of air intake model
M	Mach number
P_{mean}	time mean value of static pressure
P_0	total pressure in settling chamber
$p_{\text{p.c.}}$	static pressure in plenum chamber
P_s	static pressure
ΔP	amplitude of static pressure fluctuation
P1～P7	pressure indicators
R	radius of round-edged cowl lip

Re	Reynolds number
T	temperature
T.R.	throttle ratio ($\equiv A_E/A^*$)
T.R.*	throttle ratio at critical regime
α	angle of attack
δ_c	inclination of cowling inner wall
ϕ_1	inclination of cowling outer wall
ϕ_2	inclination of center body surface
φ_{JP}	phase relation
ρ	density
μ	viscosity
θ	azimuth angle
θ_A	inclination of line connecting between center body apex and cowl lip
θ_s	semi apex angle
θ_w	oblique shock wave angle

Notations in Appendix B

Φ	disturbance velocity potential
φ	related disturbance velocity potential
k	nondimensionalized frequency
ν	angular frequency
κ	specific heat coefficient
t	time
ξ	deviation of shock wave from the mean position

upperscript

—	nondimensionalized

subscript

m	averaged
1	ahead of shock
2	behind of shock

APPENDIX A

Summary of previous experiments for inlet buzz.

	Dimensions of S.W.T.	M	L mm	D_c (D_i) mm	l mm	d_{max}	D_c/L	θ_S	θ_A	δ_C	ϕ_1
Dailey (6)	432×508 (nonreturn)	1.96 1.90 2.0	2489 3048 3556	133 (36.6)	593	59	0.0536 0.0437 0.0375	20° 25° 30°	33° 48′ 45° 36° 54′		
Sterbentz and Evard (7)	2438×1829 (tunnel) and others (free jet)	1.50 1.60 1.70 1.77 1.80 1.90 2.00	4749 2399 1423 4755	407 203 203 407			0.085 0.1436	20° 23° 25°		4°	12°
Trimpi (9) (10)	102×137 (blow down)	1.90 1.94	864 3962 9906 3048 1524	44.5 102.3 32.5	146	17.8	0.0515 0.0112 0.0045 0.0336 0.0672	25° 30° 25°	44° 39° 50′ 40° 40′ 48° 30′ 36° 50′ 43° 40′ 43° 10′ 48° 06′ 44° 12′ 40° 06′	13°	
Hermann (11)	305×305 (blow down) 125.5×125.5 (free jet)	3.0 2.54 2.00	344	121.6			0.353	30°	39° 54′		
The authors	200×180 (blow down)	2.0	635	40	540	32.4	0.063	25°	29° 12′ 31° 36′ 35° 48′	19°24′	31°

(l; Center body length, d; Center body diameter)

APPENDIX B A Note on Inlet Buzz Characteristics

It is known from our experiments and other references that inlet buzz phenomenon has certain characteristic frequencies which are predominant to the model tested. These frequencies are close to the ones determined by the acoustic resonance theory, which suggests to able to obtain the buzz frequencies as a boundary value problem remarking two particular longitudinal boundary conditions, the inlet shock wave and the rear exit throat being choked.

1. Basic equations

As shown in Fig. B-1 the calculating model is assumed as a simple circular duct, which has no center body but an exit throat at its end, so that the flow through the model is axisymmetric. And further each flow paricle is also assumed to experience isentropic change after crossing the front shock wave.

As basic equations, continuity, momentum and energy equations are adopted together with the equation of state of perfect gas and thermodynamic relations. Only initial stage of buzz oscillation is considered, which suggests the use of small perturbation method. Taking the terms up to first order derivatives, we obtain well known wave equation for disturbance velocity potential Φ.

In cylindrical coodinates (x, r),

$$(1-M^2)\frac{\partial^2\Phi}{\partial x^2}+\frac{1}{r}\frac{\partial}{\partial r}\left(r\frac{\partial\Phi}{\partial r}\right)=\frac{1}{a_m^2}\left(\frac{\partial^2\Phi}{\partial t^2}+2U_m\frac{\partial^2\Phi}{\partial x\partial t}\right) \tag{1}$$

Now we introduce following nondimensional coordinates and variables,

$$\left.\begin{aligned} x&=L\cdot\bar{x}\\ r&=\frac{D}{\sqrt{1-M^2}}\cdot\frac{L}{D}\cdot\bar{r}\\ t&=\frac{L}{U_m}\cdot\bar{t}\\ \Phi(x,r,t)&=L\cdot U_m\cdot\bar{\Phi}(\bar{x},\bar{r},\bar{t}) \end{aligned}\right\} \tag{2}$$

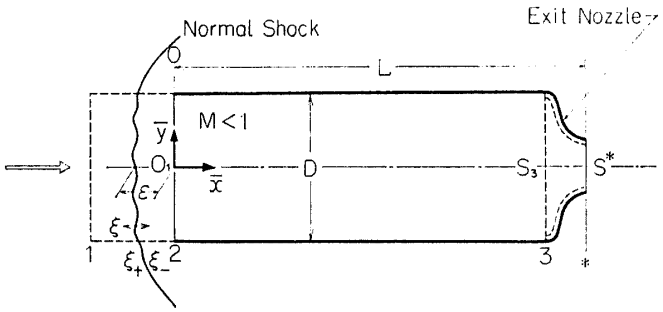

FIG. B-1. Air intake model for calculation.

$$\left.\begin{aligned} k&=\frac{\nu L}{U_m}\\ K&=\frac{kM}{1-M^2}\\ \mu&=\frac{kM^2}{1-M^2}\end{aligned}\right\} \tag{3}$$

Putting

$$\bar{\Phi}(\bar{x},\bar{r},\bar{t})=\varphi(\bar{x},\bar{r})e^{i(k\bar{t}+\mu\bar{x})} \tag{4}$$

, which means to require a harmonically oscillating solution, then we obtain a simple Helmholtz equation;

$$\frac{\partial^2\varphi}{\partial\bar{x}^2}+\frac{1}{\bar{r}}\cdot\frac{\partial}{\partial\bar{r}}\left(\bar{r}\frac{\partial\varphi}{\partial\bar{r}}\right)+K^2\varphi=0 \tag{5}$$

2. Boundary conditions

As far as inviscid small disturbance flow is assumed, four boundary conditions are just enough to get the particular frequency parameter as the eigenvalue of this oscillating system.

These boundary conditions have been derived as follows:

a) Radial boundary conditions

$$\left.\begin{aligned} &\bar{r}=0 \qquad \text{(axisymmetric)},\\ &\bar{r}=\sqrt{1-M^2}\cdot\frac{D}{2L}, \qquad \frac{\partial\varphi}{\partial\bar{r}}=0\end{aligned}\right\} \tag{6}$$

b) Longitudinal boundary conditions

$$\left.\begin{aligned} &\bar{x}=0 \qquad \text{(front shock wave condition)},\\ &i\left\{k+\left(1+\frac{1}{M^2}\cdot\frac{1}{f}\right)\mu\right\}\varphi+\left(1+\frac{1}{M^2}\cdot\frac{1}{f}\right)\frac{\partial\varphi}{\partial\bar{x}}=0\\ &\bar{x}=1 \qquad \text{(chocking condition at the rear exit)},\\ &i\left\{k+\left(1+\frac{1}{M^2}\cdot\frac{2}{\kappa-1}\right)\mu\right\}\varphi+\left(1+\frac{1}{M^2}\cdot\frac{2}{\kappa-1}\right)\frac{\partial\varphi}{\partial\bar{x}}=0\end{aligned}\right\} \tag{7}$$

Where a function f is defined as $\delta u_2=f(k,M,\varepsilon/L)\cdot\delta\rho_2$, given by solving the following equation; (Equation (8) see next page)

Here, R, U, P are functions of M, which give the relation of first order quantities through the normal shock.

3. Eigenvalue problem

Solution to Eq. (5) is easily derived as usual; $\varphi=X(\bar{x})\cdot R(\bar{r})$. Then we get from Eq. (5)

$$
\begin{bmatrix}
\dfrac{M^2-1}{1+((\kappa-1)/2)M^2}+iR\dfrac{\varepsilon}{2L}\cdot k & 0 & 1 & 4\dfrac{L}{D}\cdot\dfrac{\varepsilon}{L} \\
i(U+R)\kappa M^2\dfrac{\varepsilon}{2L}\cdot k & 1 & \kappa M^2\left(2+i\dfrac{\varepsilon}{2L}k\right) & 4\dfrac{L}{D}\cdot\dfrac{\varepsilon}{L}\cdot\kappa M^2 \\
P & 1 & 0 & -i\dfrac{\kappa M^2}{2}\cdot\dfrac{D}{L}k \\
2\dfrac{\kappa-1}{\kappa+1}(1-M^2)-i\left\{P\dfrac{1}{\kappa}+U(\kappa-1)M^2-R\right\}\dfrac{\varepsilon}{2L}\cdot k & 1+i\dfrac{1}{\kappa}\dfrac{\varepsilon}{2L}k & (\kappa-1)M^2\left(1+i\dfrac{\varepsilon}{2L}k\right) & 0
\end{bmatrix}
\times
\begin{bmatrix}
\delta\xi \\ \delta P_2 \\ \delta u_2 \\ \delta v_m
\end{bmatrix}
$$

$$
=
\begin{bmatrix}
-\left(1+i\dfrac{\varepsilon}{2L}k\right) \\
-\kappa M^2\left(1+i\dfrac{\varepsilon}{2L}k\right) \\
0 \\
1+i\dfrac{\varepsilon}{2L}k
\end{bmatrix}
\times\delta\rho_2 \qquad (8)
$$

$$\left.\begin{aligned}\frac{1}{\bar{r}}\cdot\frac{\partial}{\partial\bar{r}}\left(\bar{r}\frac{\partial R}{\partial\bar{r}}\right)+\lambda^2R=0\\ \ddot{X}+(K^2-\lambda^2)X=0\end{aligned}\right\} \tag{9}$$

Using the radial boundary conditions, we obtain

$$\varphi=\sum_{n=0}^{\infty}\varphi_n=\sum_{n=0}^{\infty}(b_1e^{i\omega_n x}+b_2e^{-i\omega_n x})\cdot J_0(\lambda_n\cdot\bar{r}) \tag{10}$$

Where λ is separation constant and $\omega_n^2=K^2-\lambda_n^2$. To satisfy the longitudinal boundary conditions, the above solution, Eq. (10), must satisfy the following relation;

$$\frac{\omega_n}{t_g\omega_n}=i\frac{(k+\alpha\mu)(k+\beta\mu)-\alpha\cdot\beta\omega_n^2}{(\alpha-\beta)k} \tag{11}$$

Where $\alpha\equiv(1+fM^2)/(fM^2)$, $\beta\equiv(1+M^2(\kappa-1)/2)/(M^2(\kappa-1)/2)$.

Given definite values of M, D/L and ε/L, the solutions for an algebraic Eq. (11) of complex variables can be calculated numerically. We used the electronic computer "HITAC 5020".

4. Results and discussion

When we find from Eq. (11) the value of k, the real part of which shows the oscillating frequency, while the imaginary part of which gives the discrimination whether the small oscillation goes to growth or damp, we can also calculate the amplitude and the phase relation of pressure fluctuation along the longitudinal direction. We take here only the case of oscillating mode of the lowest order, $\omega_n=0$, which might be considered as the most important one practically.

Taking only the term of n=0, we get

$$\frac{\Delta P(\bar{x},\bar{t})}{\Delta P(0,\bar{t})}=\frac{1/(1-M)\cdot e^{i(kM/(1-M))\bar{x}}+1/(1+M)\cdot B_0e^{-i(kM/(1-M))\bar{x}}}{1/(1-M)+1/(1+M)\cdot B_0};\ 0\leq\bar{x}\leq1 \tag{12}$$

Where

$$B_0=\frac{k+\alpha\mu-\alpha\omega_0}{k+\alpha\mu+\alpha\omega_0}=\frac{1+M(1-\alpha)}{1-M(1-\alpha)}\cdot\frac{1-M}{1+M}$$

Thus, taking the absolute value and the argument of Eq. (12), we obtain the longitudinal amplitude and phase distribution referred to those at the position $\bar{x}=0$.

To make clear the property of k depending upon M, we first consider the simplest case where $n=0$ and $\varepsilon=0$, that it, the plane mode solution with no spillage out of cowl lip. Now $\lambda_{n=0}=0$, and then we get $\omega_{n=0}=k_{n=0}\cdot M/(1-M^2)$, Re $[\omega_{n=0}]>0$.

Substituting this into Eq. (11), we get

$$\frac{1}{t_g\omega_{n=0}}=i\cdot\frac{f-2/(\kappa-1)\cdot1/M^2}{(\kappa-1)/2-f}\cdot\frac{\kappa-1}{2}\cdot M \tag{13}$$

This equation shows that real part of $\omega_{n=0}$ is not affected by M, because f becomes real function of M when $\varepsilon=0$. This fact, however, does not mean that the frequency can be independent upon M, since ν is related to ω through the parameter M. We can solve

$$\mathrm{Re}\,[\omega_{n=0}]=\frac{2m-1}{2}\pi, \qquad m=1, 2, \cdots$$

and then draw as many lines of Re $[K_{n=0}]$ as we want, corresponding to the value of m.

We can also consider the limiting cases as $M\to 1.0$ and $M\to\sqrt{(\kappa-1)/2\kappa}$. As M reaches 1.0, f becomes -1, thus we get Im $[\omega_{n=0}]\to-\infty$, which is inadequate for the case. Naturally we imagine $\omega_{n=0}=0$, which is excluded in Eq. (13). As M becomes $\sqrt{(\kappa-1)/2\kappa}$ the density behind the normal shock becomes zero, which has no physical meaning. Nevertheless, we get $f\to-\infty$ and will obtain a definite Im $[k_{n=0}]$ in this case.

Bearing this nature in mind, we numerically solve Eq. (11) and obtain some results which are shown in Figs. B-2~B-4. Fig. B-2 shows the simplest case of plane wave mode with no spillage flow, thus independent upon D/L. Characteristic frequency steadily decreases with the increase of Mach number in the air intake model whose geometrical size is fixed. There we also plot some experi-

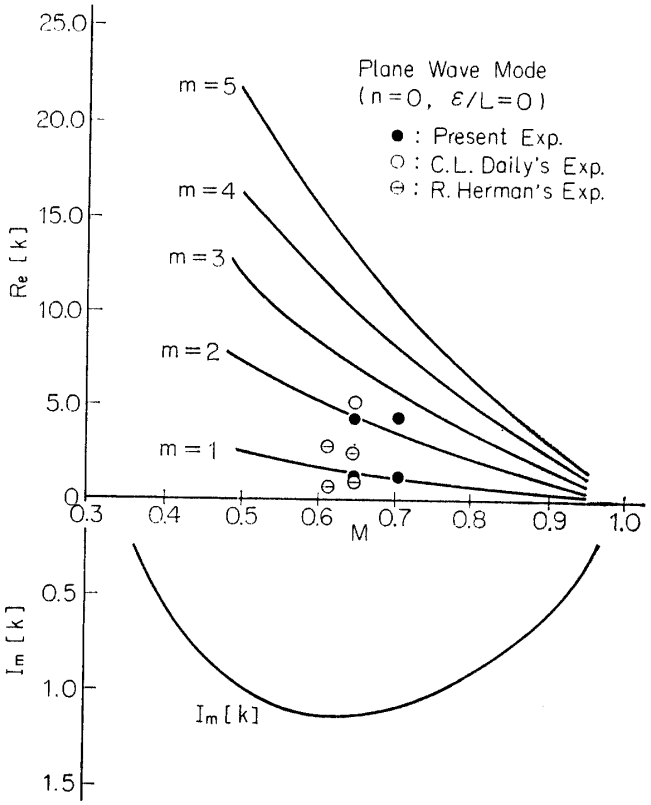

FIG. B–2. Relation between nondimensional frequency (k) of inlet buzz and Mach number (M).

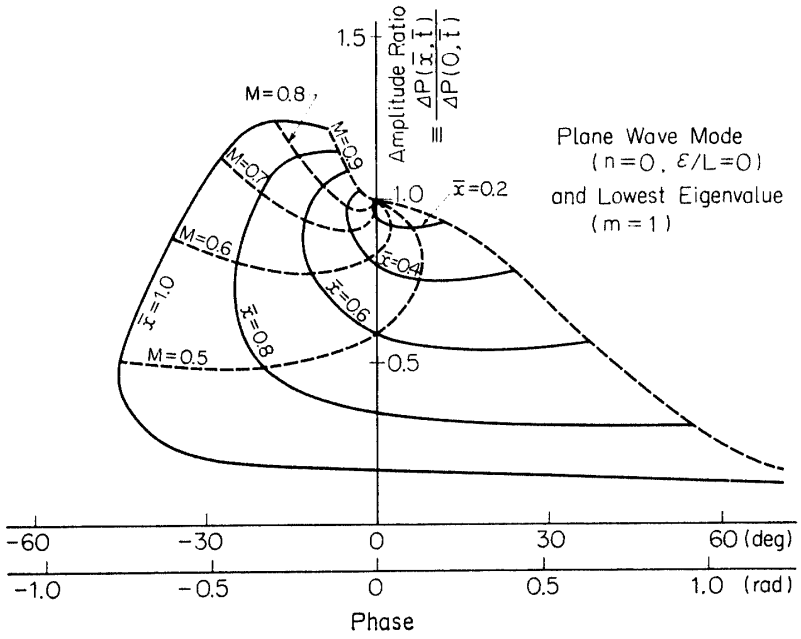

FIG. B–3. Relation between amplitude ratio of inlet buzz and its location (x) or Mach number (M).

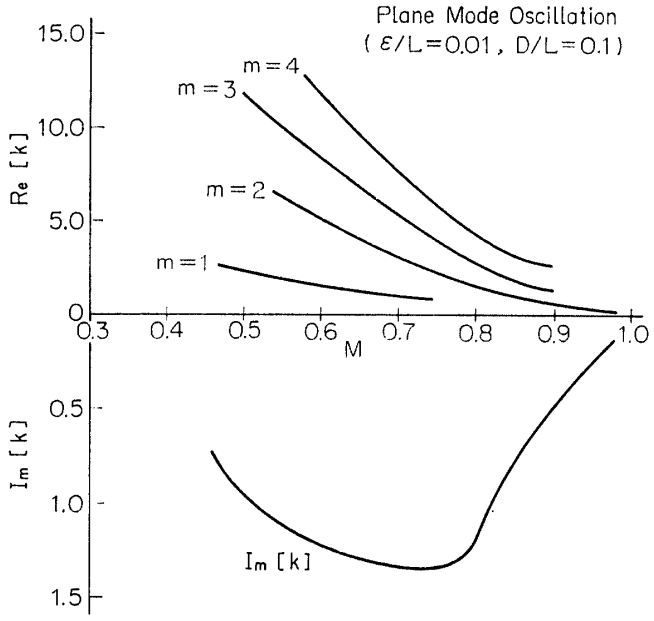

FIG. B–4. Relation between nondimensional frequency (k) of inlet buzz and Mach number (M).

mental data recalculated for our use from the previous publishment [6] and [11], together with our experimental values. As expected we obtain many values of Re [k] at a certain Mach number, and our experimental points are well on the calculated lines, the lowest and the next above it. This fact might be used to explain the appearance of two or more buzz characteristic frequencies as the throttle ratio is varied in our experiments. As shown in Fig. B-2, however, the

imaginary values of k are all positive, which means that any oscillations become always damped, thus the theory contradicts to the actual phenomenon observed through experiments. It is seen therefore that the model assumed without the center body for calculation is inadequate to examine the buzz characteristics, although the measured frequencies are well on the calculated lines as described just above.

In Fig. B–3 is shown a result of the amplitude and phase distribution on the left hand of Eq. (12) only for the lowest eigenvalue ($m=1$). From this figure we can find the location and the Mach number of the maximum amplitude with the phase angle. Fig. B–4 shows the result for the case of a plane mode oscillation when the detached shock wave distance $\varepsilon/L=0.01$ and the diameter-length ratio $D/L=0.1$. In spite of the introduction of ε, the results are just slightly deviated towards the stable tendency from the ones of the case $\varepsilon=0$.

Finally, let us see the effect of the presence of the center body without any essential change to the previous procedure. Now the boundary conditions are all same as the case without the center body, only except the condition of the axis line ($\bar{r}=0$) may be replaced by $\partial\varphi/\partial\bar{r}=0$ at $\bar{r}=C\cdot\bar{r}$, where C is the ratio of center body diameter to the outer cylinder ($0<C<1$). According to the results calculated under the above boundary conditions, the effect of the presence of the center body is little, if C is small compared with 1.0. In our experimental model, $C\simeq 0.8$, it seems to be very difficult to assume the value of C as negligible small. In addition, the presence of the center body can be discussued from another point of view, that is, the decreasing of the Mach number coming into the inlet duct system, which seems to give large effect on k as seen in Fig. B–2 and B–4.

5. Conclusion

A theory was proposed emphasizing two boundary conditions, the front shock wave condition and the rear choked exit, where the possibility to explain the appearance of more than one characteristic buzz frequencies is shown. The theory predicts:

1) Characteristic frequencies steadily increase with the decrease of the Mach number in the air intake model whose geometrical size is fixed.

2) It is satisfactory to examine the buzz phenomenon, particularly for its frequency, by one dimensional model, provided the inlet Mach number does not become near 1.0 and the center body diameter is not so large compared with the cowling diameter.

3) The effect of the presence of center body on the buzz characteristics may be viewed from the very sense that it decreases the inlet Mach number.

However, the theory is completely inadequate to explain the instability of the system, which remains to be examined furthermore in the future.